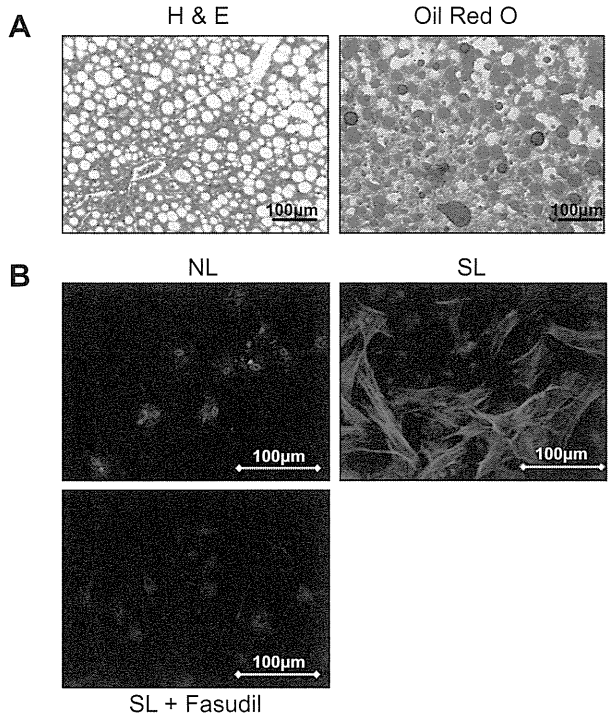

Fig. 1. Oil red O staining and morphology changes of HSCs isolated from rat SL. (A) Representative H&E- and oil red O-stained sections. Rats fed a choline-deficient diet for 6 weeks had more than 60% of macrovesicular steatosis. (B) Images show differences in F-actin expression in isolated HSCs from NL, SL, and SL treated with fasudil (10 μM, 24 h). Cells were stained to show F-actin (red) and nuclei (blue). HSCs isolated from NL showed slight stress fiber formation and F-actin expression. By contrast, HSCs isolated from SL had an elongated, fusiform morphology with prominent dendritic processes. Fasudil suppressed both stress fiber formation and F-actin expression. (For interpretation of the references to colour in this figure legend, the reader is referred to the web version of this article.)

significantly smaller than those with HSCs-NL (p <0.01). In the presence of fasudil (10 μM), this reduction in the areas of gels with HSCs-SL was not observed. The gel areas containing HSCs-SL were significantly smaller in the presence of ET-1 (5 nM) than those with HSCs-SL in the absence of ET-1 (p <0.01). In sharp contrast, however, when fasudil was added to the culture medium in the presence of ET-1, the shrinkage of the gels with HSCs-SL was suppressed (p <0.01; Fig. 2A and B). Furthermore, the NO synthase inhibitor L-NAME (100 μM) was used to investigate the influence of NO on HSCs. Fasudil suppressed the contraction of HSCs-SL even in the presence of L-NAME (p <0.01; Fig. 2C and D).

Expression of ROCK2 and phosphorylation of MLC and cofilin

To examine the possible involvement of the Rho/ROCK pathway in the activation of HSCs, the expression of ROCK2 and the phosphorylation state of MLC and cofilin, a downstream effector of Rho/ROCK signaling, were assessed by Western blot analysis with monoclonal antibodies to ROCK2 and the phosphorylated form of MLC and cofilin. Quantitative analysis using a scanning densitometer confirmed that ROCK2 was significantly overexpressed in HSCs-SL compared with HSCs-NL (p <0.01) (Fig. 3A). The phosphorylation level of MLC in HSCs-SL was significantly increased compared with that in HSCs-NL. The phosphorylation levels of MLC and cofilin were significantly enhanced by ET-1 in HSCs-SL

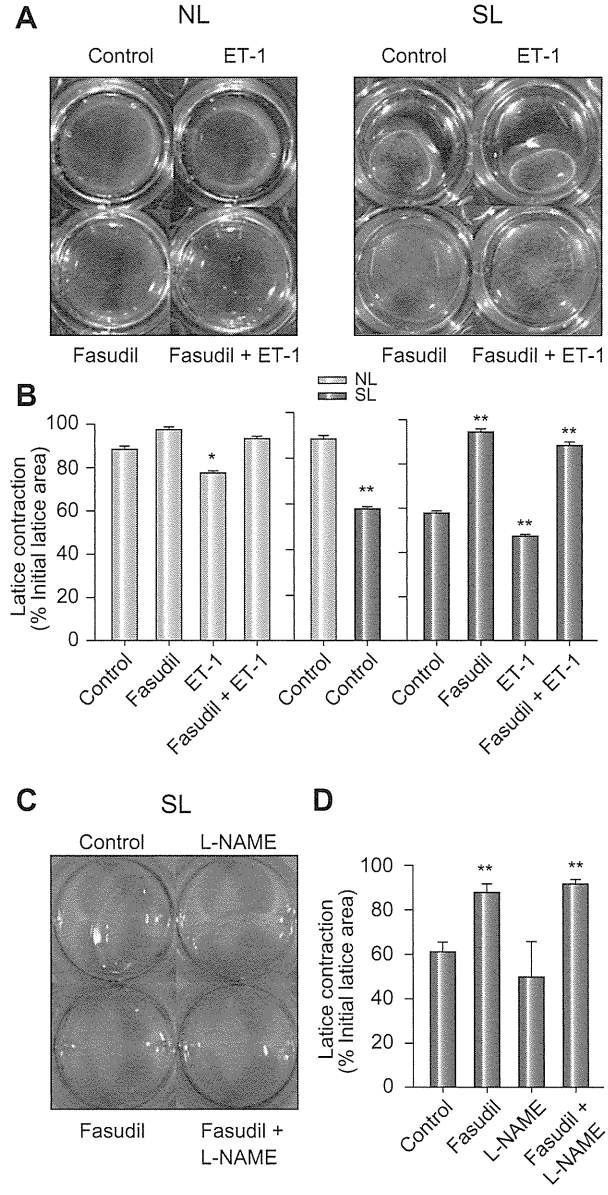

Fig. 2. Collagen gel contraction assay. (A) Contraction of collagen gels induced by the activation of isolated HSCs in untreated NL and SL, and in NL and SL treated with ET-1, fasudil or a combination of the two. Without the addition of HSCs, the collagen gels did not contract during the observation period (not shown). Control, medium alone; ET-1, 5 nM ET-1; Fasudil, 10 μM fasudil; Fasudil + ET-1, 10 μM fasudil and 5 nM ET-1. (C) Contraction of collagen gels in SL and SL treated with L-NAME, fasudil or a combination of the two. Control, medium alone; L-NAME, 100 μM L-NAME; Fasudil, 10 μM fasudil; Fasudil + L-NAME, 10 μM fasudil, and 100 μM L-NAME. (B and D) Changes in the collagen gel area induced by contraction of HSCs. HSCs isolated from rat NL, closed bars; HSCs isolated from rat SL, open bars. Average values (SD) of three independent experiments are shown. *p <0.05 compared to each control; **p <0.01 compared to each control.

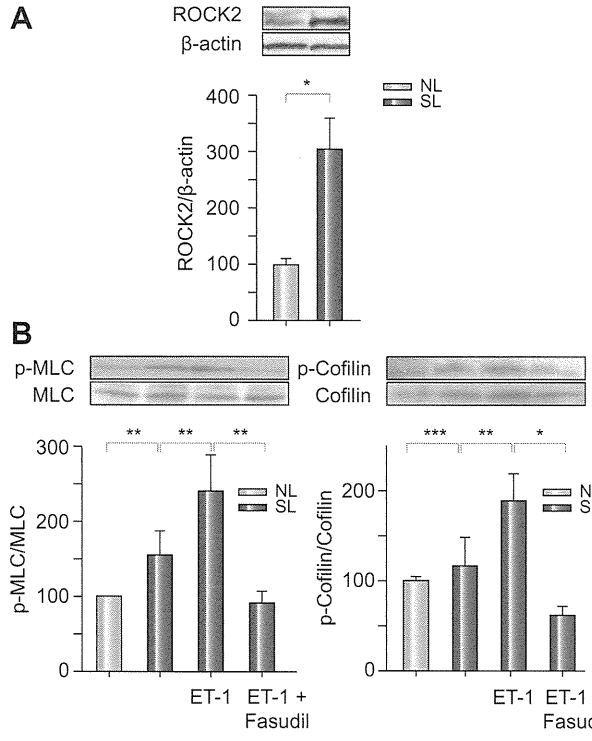

Fig. 3. Western blot analyses in rat HSCs isolated from rat NL or SL. (A) Expression level of ROCK2. (B) Total and phosphorylated MLC and cofilin. HSCs isolated from rat SL were either left untreated or cultured with 10 μM fasudil and/or 5 nM ET-1 for 30 min. The protein expression of ROCK2 was normalized to the level of β-actin. The phosphorylation levels of MLC and cofilin were normalized to total MLC and cofilin protein expression, respectively. Each figure is representative of three independent experiments. Average values (SD) for individual groups are shown. *p <0.01, **p <0.05, ***N.S.

(p <0.05, in both), but the effects were suppressed by fasudil (p <0.05, 0.01, respectively; Fig. 3B).

Influence of IR on the secretion of ET-1

Serum ET-1 concentrations were measured after 30 min of ischemia followed by 3 h of reperfusion using ELISA. Serum ET-1 concentrations significantly increased after IR in rats with NL (p <0.01). Serum ET-1 concentrations after IR were significantly higher in rats with SL than in rats with NL (p <0.01). Furthermore, fasudil significantly suppressed the serum ET-1 concentrations after IR (p <0.01; Fig. 4).

Influence of IR on portal perfusion pressure

To determine the influence of IR on the microvascular blood flow in the hepatic lobule, the portal perfusion pressure was assessed in isolated rat livers. Perfusion pressures were measured after 45 min of ischemia followed by 15 min of reperfusion. The portal perfusion pressures in rats with SL were significantly higher than those in rats with NL (p <0.05). The portal perfusion pressures in rats with SL after IR were significantly higher than those in rats with SL that did not undergo IR (p <0.01), and the effect was suppressed by fasudil (p <0.01; Fig. 5).

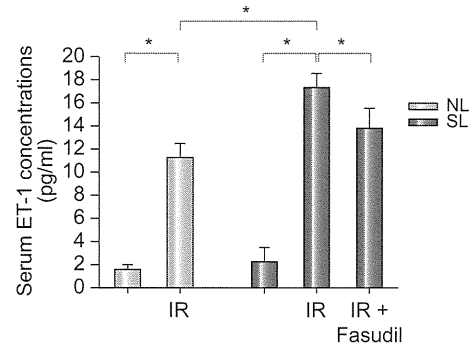

Fig. 4. Serum ET-1 concentrations, reflecting secretion from SECs and HSCs. Blood samples were collected from rats with NL or SL after 30 min of ischemia followed by 3 h of reperfusion. A group of the SL rats received fasudil (10 mg/kg) 30 min before ischemia. Average values (SD) for individual groups are shown; for all groups, n = 6. *p <0.01.

Biochemical assessment, histological study, and survival rates after IR

AST and ALT are well-established markers of hepatocellular injury after IR. Serum AST and ALT levels were measured after 30 min of ischemia followed by 3 or 24 h of reperfusion. The increase in AST at 3 and 24 h and in ALT at 3 h after IR of the untreated rats with SL was significantly higher than in fasudil-treated rats with SL (Fig. 6A). For histological analysis, liver specimens were obtained after 45 min of ischemia followed by 24 h of reperfusion. Liver specimens from untreated rats with SL after IR showed distortion of architecture, sinusoidal congestion, microthrombus, and extensive areas of coagulative necrosis. In contrast, specimens from the SL group treated with 10 mg/kg fasudil showed almost normal hepatic structure (Fig. 6B). TUNEL staining of liver tissue sections after IR showed that most hepatocytes in NL were TUNEL positive, whereas only minimal TUNEL staining was found in SL (Supplementary Fig. 2). The survival rate of rats with SL that underwent 45 min of ischemia was significantly lower than that of rats with NL (p <0.01). However, treat-

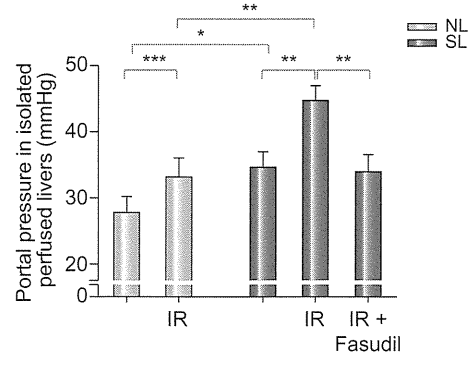

Fig. 5. Portal pressures in isolated perfused livers from rats with NL and SL. Livers were untreated, treated with 45 min of ischemia followed by 15 min of reperfusion, or preinjected with 10 mg/kg fasudil intraperitoneally 30 min before IR. Average values (SD) for individual groups are shown; for all groups, n = 5. *p <0.05; **p <0.01, ***N.S.

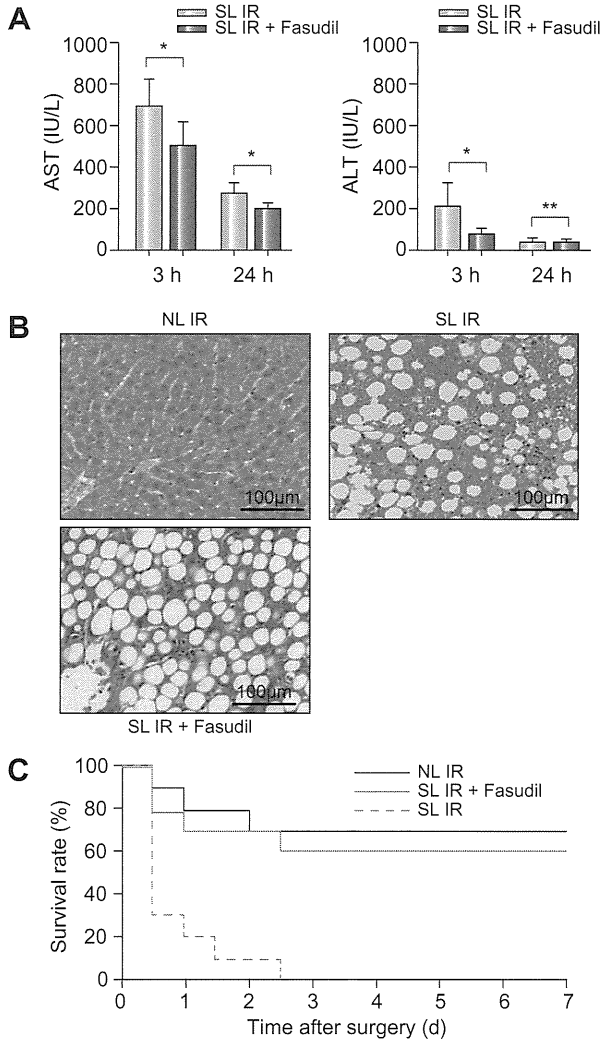

Fig. 6. Influence of IR in rats with SL. Rats with NL or SL were treated with IR. A fraction of the SL group received fasudil (10 mg/kg) 30 min before IR. (A) Serum levels of AST and ALT in rats with SL after 30 min of ischemia followed by 3 and 24 h of reperfusion. Average values (SD) for individual groups are shown; for all groups, n = 5. *p <0.05, **N.S. (B) Histological examination of NL and SL after 45 min of ischemia followed by 24 h of reperfusion. Liver specimens from untreated rats with SL showed severe fat accumulation, distortion of architecture, sinusoidal congestion, and extensive areas of coagulative necrosis. Liver specimens from the group that received fasudil similarly showed severe fat accumulation but had a nearly normal hepatic structure and minimal sinusoidal enlargement in the hepatic lobule center compared with the untreated SL. Representative H&E-stained liver sections. (C) The survival rates of rats with NL or SL that underwent 45 min of ischemia. Although the survival rate of the SL group was significantly lower than that of the NL group (p <0.01), fasudil treatment significantly improved the survival rate of the SL group (p <0.01), n = 10.

ment with fasudil significantly improved the survival rate of rats with SL after IR (p <0.01; Fig. 6C).

Discussion

The SL is known to be vulnerable to IR compared with the NL. The present study is the first report to provide evidence of the effect of Rho/ROCK signaling activation in HSCs on the increased susceptibility of SL to IR injury in rats. The present results showed that the activation of HSCs in SL was associated with the upregulation of ROCK2 and that the enhanced activation of ROCK2 was involved in the induction of IR injury in SL. The intra-abdominal infusion of fasudil, a specific inhibitor of ROCK, significantly alleviated IR injury in SL.

ROCK is a downstream effector of the small GTPase Rho involved in the regulation of cytoskeletal rearrangements and cell migration. ROCK is involved in the contraction of activated HSCs, which play an important role in regulating hepatic microcirculation. Intrahepatic upregulation of ROCK contributes to increased intrahepatic resistance in cirrhotic rats and to an increased sensitivity of cirrhotic livers to vasoconstrictors [24].

In the current study, HSCs-SL showed greater stress fiber formation and overexpression of ROCK compared with NL. The contractility of the HSCs and the phosphorylation of MLC in the HSCs were significantly enhanced in SL compared with NL. These results indicated a significant activation of the HSCs-SL compared with the HSCs-NL. There have been few studies using HSCs-SL. However, liver biopsy specimens from SL and nonalcoholic steatohepatitis showed the presence of activated HSCs, identified immunohistologically using a specific monoclonal antibody to detect cytoplasmic α-smooth muscle actin, which is not present in quiescent cells. These findings revealed a correlation between the degree of HSC activation and hepatic fibrosis, and the study of these specimens suggested a trend toward increased HSC activation with increasing fat accumulation, although this lacked statistical significance [15–17]. The hepatic expression of ROCK has been shown to be elevated in livers from cirrhotic rats and patients with alcohol-induced cirrhosis, and intrahepatic upregulation of ROCK contributes to portal hypertension via an increase in hepatic vascular resistance [24]. These results indicate that the activation of HSCs may be related to the overexpression of ROCK.

In our previous report using normal rat livers, the IR-induced impairment of sinusoidal microcirculation resulted, in part, from the contraction of HSCs, and Y-27632, a specific ROCK inhibitor, suppressed the IR-induced microcirculatory disturbance by promoting the relaxation of HSCs [9].

In the present study, the portal perfusion pressure was significantly increased in SL compared with NL. The perfusion pressure in SL was further increased after IR, and fasudil significantly suppressed this pressure increase. Serum ET-1 concentration was also significantly elevated after IR, and the increase in ET-1 concentration was suppressed by the administration of fasudil. These findings indicate that fasudil attenuates microvascular injury following ischemia reperfusion in SL. ET-1, which activates the Rho/ROCK pathway and elevates portal pressure via contraction of HSCs, was used as an alternative marker for IR injury in our *in vitro* studies (including a collagen gel contraction assay and measurement of MLC and cofilin phosphorylation in HSCs). This was done because it was extremely difficult to isolate HSCs from rats with SL undergoing IR owing to insufficient perfusion of pronase and collagenase, and even when successful, the isolated HSCs showed very low viability for use in further *in vitro* studies.

The contractility of the HSCs and the phosphorylation of MLC and cofilin were significantly enhanced by ET-1 in the HSCs-SL, and fasudil attenuated these effects. Furthermore, fasudil prolonged the survival of rats with SL undergoing IR and attenuated

sinusoidal congestion and hepatocyte necrosis. These results indicate that fasudil, a specific ROCK inhibitor, suppresses IR-induced liver injury by ameliorating the hemodynamic disturbance through the modulation of Rho signaling in SL, which is more vulnerable to IR than NL.

Fasudil was used as a ROCK inhibitor in the present study based on the clinical application of the inhibitor for the release of cerebral vasospasm after subarachnoid hemorrhage [25]. Fasudil was administered at a dose of 10 mg/kg by intraperitoneal injection before IR because the area under the serum fasudil concentration curve for rats after the intraperitoneal injection of the inhibitor (10 mg/kg) was 4490 ng h/ml, which was almost compatible or slightly higher than that of fasudil in humans [26]. The use of fasudil may be a new therapeutic strategy to prevent hepatic IR injury.

The results of the current study indicated that the effect of fasudil on the contractility of HSCs-SL was mediated by the direct inhibition of ROCK, and independent of the NO effect in HSCs. Anegawa *et al.* reported that in a rat model of secondary biliary cirrhosis bile duct ligation, ROCK activation with resultant eNOS activation was substantially involved in the pathogenesis of portal hypertension. Moreover, fasudil significantly suppressed ROCK activity and increased eNOS phosphorylation through a reduction of the binding of serine/threonine Akt to ROCK and an increase of the binding of Akt to eNOS [27]. The improvement of hepatic hemodynamics by fasudil has been shown to be mediated by an enhancement of NO production by sinusoidal endothelial cells (SECs), rather than by direct inhibition of Rho-kinase in HSCs. Our result was not compatible with Anegawa's report. This may be due to differences in the experimental model used. We used a collagen gel contraction assay to show that the effect of fasudil on the contractility of HSCs-SL was mediated by direct inhibition of ROCK, while in the study by Anegawa *et al.*, a bile duct ligation-induced secondary biliary cirrhosis model revealed that the hemodynamic effects of the *in vivo* administration of fasudil were associated with the production of NO by SECs, and not by direct inhibition of ROCK. The relationship between SL and NO synthesis remains to be elucidated, and further investigation is necessary. In addition, ROCK inhibitors have been reported to improve the VLDL transport functions of hepatocytes in SL, which might be one of the mechanisms underlying their protective effect against IR injury [28].

In summary, activation of Rho/ROCK signaling in HSCs-SL is associated with an increased susceptibility to IR injury. Inhibition of ROCK attenuates the activation of the HSCs-SL and improves IR injury in rats with liver steatosis.

Acknowledgments

The authors thank Asahi Kasei Co., Tokyo, Japan, for providing fasudil. This work was supported in part by a Grant-in-Aid for Scientific Research (KAKENHI 21591748 [to H.T.]) from the Ministry of Education, Science, Sports, and Culture of Japan.

Conflict of interest

The authors who have taken part in this study declared that they do not have anything to disclose regarding funding or conflict of interest with respect to this manuscript.

Supplementary data

Supplementary data associated with this article can be found, in the online version, at doi:10.1016/j.jhep.2011.04.029.

References

[1] McCormack L, Petrowsky H, Jochum W, Furrer K, Clavien PA. Hepatic steatosis is a risk factor for postoperative complications after major hepatectomy: a matched case-control study. Ann Surg 2007;245:923–930.
[2] Gomez D, Malik HZ, Bonney GK, Wong V, Toogood GJ, Lodge JP, et al. Steatosis predicts postoperative morbidity following hepatic resection for colorectal metastasis. Br J Surg 2007;94:1395–1402.
[3] Trevisani F, Colantoni A, Caraceni P, Van Thiel DH. The use of donor fatty liver for liver transplantation: a challenge or a quagmire? J Hepatol 1996;24:114–121.
[4] Hui AM, Kawasaki S, Makuuchi M, Nakayama J, Ikegami T, Miyagawa S. Liver injury following normothermic ischemia in steatotic rat liver. Hepatology 1994;20:1287–1293.
[5] Wada K, Fujimoto K, Fujikawa Y, Shibayama Y, Mitsui H, Nakata K. Sinusoidal stenosis as the cause of portal hypertension in choline deficient diet induced fatty cirrhosis of the rat liver. Acta Pathol Jpn 1974;24:207–217.
[6] Caraceni P, Ryu HS, Subbotin V, De Maria N, Colantoni A, Roberts L, et al. Rat hepatocytes isolated from alcohol-induced fatty liver have an increased sensitivity to anoxic injury. Hepatology 1997;25:943–949.
[7] Seifalian AM, Chidambaram V, Rolles K, Davidson BR. In vivo demonstration of impaired microcirculation in steatotic human liver grafts. Liver Transpl Surg 1998;4:71–77.
[8] Zhang JX, Bauer M, Clemens MG. Vessel- and target cell-specific actions of endothelin-1 and endothelin-3 in rat liver. Am J Physiol 1995;269.
[9] Mizunuma K, Ohdan H, Tashiro H, Fudaba Y, Ito H, Asahara T. Prevention of ischemia-reperfusion-induced hepatic microcirculatory disruption by inhibiting stellate cell contraction using rock inhibitor. Transplantation 2003;75:579–586.
[10] Ankoma-Sey V, Wang Y, Dai Z. Hypoxic stimulation of vascular endothelial growth factor expression in activated rat hepatic stellate cells. Hepatology 2000;31:141–148.
[11] Hirose M, Ishizaki T, Watanabe N, Uehata M, Kranenburg O, Moolenaar WH, et al. Molecular dissection of the Rho-associated protein kinase (p160ROCK)-regulated neurite remodeling in neuroblastoma N1E–115 cells. J Cell Biol 1998;141:1625–1636.
[12] Maekawa M, Ishizaki T, Boku S, Watanabe N, Fujita A, Iwamatsu A, et al. Signaling from Rho to the actin cytoskeleton through protein kinases ROCK and LIM-kinase. Science 1999;285:895–898.
[13] Kimura K, Ito M, Amano M, Chihara K, Fukata Y, Nakafuku M, et al. Regulation of myosin phosphatase by Rho and Rho-associated kinase (Rho-kinase). Science 1996;273:245–248.
[14] Amano M, Chihara K, Kimura K, Fukata Y, Nakamura N, Matsuura Y, et al. Formation of actin stress fibers and focal adhesions enhanced by Rho-kinase. Science 1997;275:1308–1311.
[15] DeLeve LD, Wang X, Kanel GC, Atkinson RD, McCuskey RS. Prevention of hepatic fibrosis in a murine model of metabolic syndrome with nonalcoholic steatohepatitis. Am J Pathol 2008;173:993–1001.
[16] Washington K, Wright K, Shyr Y, Hunter EB, Olson S, Raiford DS. Hepatic stellate cell activation in nonalcoholic steatohepatitis and fatty liver. Hum Pathol 2000;31:822–828.
[17] Reeves HL, Burt AD, Wood S, Day CP. Hepatic stellate cell activation occurs in the absence of hepatitis in alcoholic liver disease and correlates with the severity of steatosis. J Hepatol 1996;25:677–683.
[18] Elinav E, Ali M, Bruck R, Brazowski E, Phillips A, Shapira Y, et al. Competitive inhibition of leptin signaling results in amelioration of liver fibrosis through modulation of stellate cell function. Hepatology 2009;49:278–286.
[19] Sohail MA, Hashmi AZ, Hakim W, Watanabe A, Zipprich A, Groszmann RJ, et al. Adenosine induces loss of actin stress fibers and inhibits contraction in hepatic stellate cells via Rho inhibition. Hepatology 2009;49:185–194.
[20] Ushitora Y, Tashiro H, Ogawa T, Tanimoto Y, Kuroda S, Kobayashi T, et al. Suppression of hepatocellular carcinoma recurrence after rat liver transplantation by FTY720, a sphingosine-1-phosphate analog. Transplantation 2009;88:980–986.
[21] Ikeda H, Nagashima K, Yanase M, Tomiya T, Arai M, Inoue Y, et al. Sphingosine 1-phosphate enhances portal pressure in isolated perfused liver via S1P2 with Rho activation. Biochem Biophys Res Commun 2004;320:754–759.

[22] van der Heijden M, Versteilen AM, Sipkema P, van Nieuw Amerongen GP, Musters RJ, Groeneveld AB. Rho-kinase-dependent F-actin rearrangement is involved in the inhibition of PI3-kinase/Akt during ischemia-reperfusion-induced endothelial cell apoptosis. Apoptosis 2008;13:404–412.
[23] Selzner M, Rudiger HA, Sindram D, Madden J, Clavien PA. Mechanisms of ischemic injury are different in the steatotic and normal rat liver. Hepatology 2000;32:1280–1288.
[24] Zhou Q, Hennenberg M, Trebicka J, Jochem K, Leifeld L, Biecker E, et al. Intrahepatic upregulation of RhoA and Rho-kinase signalling contributes to increased hepatic vascular resistance in rats with secondary biliary cirrhosis. Gut 2006;55:1296–1305.
[25] Suzuki Y, Shibuya M, Satoh S, Sugimoto Y, Takakura K. A postmarketing surveillance study of fasudil treatment after aneurysmal subarachnoid hemorrhage. Surg Neurol 2007;68:126–131.
[26] Satoh S, Utsunomiya T, Tsurui K, Kobayashi T, Ikegaki I, Sasaki Y, et al. Pharmacological profile of hydroxy fasudil as a selective rho kinase inhibitor on ischemic brain damage. Life Sci 2001;69:1441–1453.
[27] Anegawa G, Kawanaka H, Yoshida D, Konishi K, Yamaguchi S, Kinjo N, et al. Defective endothelial nitric oxide synthase signaling is mediated by rho-kinase activation in rats with secondary biliary cirrhosis. Hepatology 2008;47:966–977.
[28] Kitamura K, Tada S, Nakamoto N, Toda K, Horikawa H, Kurita S, et al. Rho/Rho kinase is a key enzyme system involved in the angiotensin II signaling pathway of liver fibrosis and steatosis. J Gastroenterol Hepatol 2007;22:2022–2033.

Suppression of immune responses by nonimmunogenic oligodeoxynucleotides with high affinity for high-mobility group box proteins (HMGBs)

Hideyuki Yanai[a,b,1], Shiho Chiba[a,1], Tatsuma Ban[a,1], Yukana Nakaima[a], Takashi Onoe[c], Kenya Honda[a,d], Hideki Ohdan[c], and Tadatsugu Taniguchi[a,b,2]

[a]Department of Immunology, Graduate School of Medicine and Faculty of Medicine, University of Tokyo, Tokyo 113-0033, Japan; [b]Core Research for Evolution Science and Technology, Japan Science and Technology Agency, Tokyo 102-0075, Japan; [c]Department of Surgery, Division of Frontier Medical Science, Graduate School of Biomedical Sciences, Hiroshima University, Hiroshima 734-8551, Japan; and [d]Precursory Research for Embryonic Science and Technology, Japan Science and Technology Agency, Saitama 332-0012, Japan

Contributed by Tadatsugu Taniguchi, May 27, 2011 (sent for review May 13, 2011)

The activation of innate immune responses by nucleic acids is central to the generation of host responses against pathogens; however, nucleic acids can also trigger the development and/or exacerbation of pathogenic responses such as autoimmunity. We previously demonstrated that the selective activation of nucleic acid-sensing cytosolic and Toll-like receptors is contingent on the promiscuous sensing of nucleic acids by high-mobility group box proteins (HMGBs). From this, we reasoned that nonimmunogenic nucleotides with high-affinity HMGB binding may function as suppressing agents for HMGB-mediated diseases, particularly those initiated and/or exacerbated by nucleic acids. Here we characterize an array of HMGB-binding, nonimmunogenic oligodeoxynucleotides (ni-ODNs). Interestingly, we find that binding affinity is rather independent of nucleotide sequence, but is instead dependent on length and structure of the deoxyribose backbone. We further show that these ni-ODNs can strongly suppress the activation of innate immune responses induced by both classes of nucleic acid-sensing receptors. We also provide evidence for the suppressive effect of an ni-ODN, termed ISM ODN, on the induction of adaptive immune responses and in mouse models of sepsis and autoimmunity. We discuss our findings in relation to the critical role of HMGBs in initiating immune responses and the possible use of these ni-ODNs in therapeutic interventions.

pattern recognition receptors | retinoic acid-inducible gene I-like receptor | experimental autoimmune encephalomyelitis

The innate immune system is integral to the protection of the host against invading pathogens by providing immediate defense and the subsequent activation of the adaptive immune system. Pattern recognition receptors (PRRs) are germ line-encoded receptors that recognize conserved pathogen-associated molecular patterns (PAMPs) and potently activate cells of the innate immune system (1, 2). The protective role of PRRs against infectious microbial pathogens via the induction of adaptive immunity has been unequivocally demonstrated; however, the activation of these receptors may also result in eliciting harmful immune responses such as life-threatening inflammation and autoimmunity (3, 4). During microbial infection or tissue damage, DNA and RNA potently activate the innate and subsequent adaptive immune responses. In mammals, the transmembrane PRR Toll-like receptor (TLR)3, TLR7, and TLR9, respectively, recognize double-stranded RNA, single-stranded and short double-stranded RNAs, and hypomethylated DNA, whereas retinoic acid-inducible gene I (RIG-I)-like receptors, namely RIG-I and melanoma differentiation-associated gene 5 (MDA5), are best known as RNA-sensing receptors in the cytosol, but more recently have been shown to also participate in the cytosolic DNA-sensing system (5–8). In addition, cytosolic DNA-sensing receptors, which include DNA-dependent activator of IFN regulatory factors (IRFs) (DAI), absent in melanoma 2 (AIM2), among others, have been identified (9, 10). The hallmark of the innate immune responses activated by these receptors is the induction of type I IFNs, proinflammatory cytokines, and chemokines, except for AIM2, which induces the inflammasome (6, 10).

We showed previously that high-mobility group box proteins (HMGB1, 2, and 3) are essential for triggering all nucleic acid receptor-mediated innate immune responses (11). Indeed, HMGBs bind to various immunogenic nucleic acids in vitro, and cells in which the expression of HMGBs is suppressed exhibit a profound defect in their ability to evoke innate immune responses, indicating a hierarchy in the nucleic acid-mediated activation of immune responses wherein the selective activation of nucleic acid-sensing receptors is contingent on the more promiscuous sensing of nucleic acids by HMGBs. In addition, HMGB1 is secreted by innate immune cells in response to PAMPs and released by injured or dying cells, and transmits signals to the cell interior via the activation of receptors that include TLR4, thereby occupying a crucial role in the pathogenesis of both sterile and infectious inflammations (12–14). In this context, numerous antagonists that neutralize HMGB1 in preclinical disease models have supported the role of HMGB1 in regulating innate and adaptive immune responses in health and during inflammatory diseases such as arthritis, sterile ischemia/reperfusion injury, cancer, and infection (15, 16). Thus, selectively targeting HMGB1 and its family members may be of clinical use and could provide key insights into the pathogenesis of various inflammation-associated diseases.

In view of our previous findings that HMGBs bind nucleic acids promiscuously, we searched for nonimmunogenic oligodeoxynucleotides (ni-ODNs) showing high-affinity HMGB binding with the rationale that such nucleotides may effectively suppress HMGB-associated diseases initiated and/or exacerbated by nucleic acids. Here we introduce an array of ni-ODNs that can strongly bind to HMGBs, which we find depends on their length and phosphorothioate deoxyribose backbone. We also show an inhibitory effect of an ni-ODN in the induction of adaptive immune responses as well as in animal disease models associated with HMGBs, and discuss the significance of our findings from a therapeutic point of view.

Results

Generation of ni-ODNs with High-Affinity Binding to HMGBs. On the basis of our previous finding that the TLR9 agonist CpG-B ODN shows a markedly high affinity with HMGBs (11), we rational-

Author contributions: H.Y., S.C., T.B., K.H., H.O., and T.T. designed research; H.Y., S.C., T.B., Y.N., and T.O. performed research; T.O. and H.O. contributed new reagents/analytic tools; H.Y., S.C., T.B., and T.T. analyzed data; and H.Y., S.C., T.B., K.H., and T.T. wrote the paper.

The authors declare no conflict of interest.

[1]H.Y., S.C., and T.B. contributed equally to this work.

[2]To whom correspondence should be addressed. E-mail: tada@m.u-tokyo.ac.jp.

This article contains supporting information online at www.pnas.org/lookup/suppl/doi:10.1073/pnas.1108535108/-/DCSupplemental.

ized that analogs without the CpG motif may also show similar if not higher affinities with HMGBs but, unlike CpG-B ODN, which activates TLR9 (5), will be nonimmunogenic (17). Thus, we generated ODNs carrying GpG or GpC in lieu of the CpG dinucleotide sequence of CpG-B ODN (Fig. S1*A*), respectively termed ISM ODN and ISR ODN, and then examined their interaction with HMGBs with these ODNs by competitive pull-down assay: In this assay, inhibition of the precipitation of a recombinant HMGB protein by biotin-conjugated CpG-B ODN was monitored by increasing the amounts of unconjugated ODN of interest (11). As expected, the precipitation of HMGB1 was inhibited by unconjugated CpG-B ODN in a dose-dependent manner, whereas ISM and ISR ODNs also showed inhibition in this assay (Fig. 1*A*). Among the three ODNs examined, the half-maximal inhibitory concentration (IC_{50}) was lowest for ISM ODN, suggesting that ISM ODN has the highest affinity with HMGB1 (Fig. 1*A*). Unlike CpG-B ODN, ISM and ISR ODNs were inert in evoking innate immune responses on the basis of cytokine induction in dendritic cells (DCs) (Fig. S1*B*).

Because these ODNs all have a phosphorothioate backbone instead of the usual phosphodiester backbone (11), we next asked whether the nature of the sugar backbone would affect ODN affinity with HMGB1 by generating an ISM ODN with a natural phosphodiester bond, termed PD-ISM ODN. When PD-ISM ODN was subjected to the pull-down assay, the inhibition of HMGB1–CpG-B ODN interaction was not observed, indicating that the phosphorothioate backbone is a critical element for ODN binding to HMGB1 (Fig. 1*B*). However, because the inhibition of HMGB1 precipitation by a base-free phosphorothioate deoxyribose homopolymer, termed PS (18), is far weaker than the inhibition by CpG-B ODN and ISM and ISR ODNs of identical length, it is clear that the bases also contribute to HMGB1 binding (Fig. 1*B*).

The above observations prompted us to examine whether the base sequence and length of ODNs affect their binding to HMGB1 by generating various lengths of poly(dA) with the phosphorothioate backbone (Fig. S1*C*). As shown in Fig. 1*C*, 20-mer poly (dA) (A20 ODN) inhibited the binding of HMGB1 to CpG-B ODN, but the inhibition was much weaker for 15-mer poly(dA) (A15 ODN), whereas 10- and 5-mer poly(dA) (A10 and A5 ODNs, respectively) failed to inhibit the CpG-B ODN–HMGB1 interaction entirely. Essentially the same observations were made when poly(dC) ODNs (C20, C15, C10, and C5 ODNs) were similarly examined (Fig. S1*D*). These observations thus identify three critical elements of ODNs for their high-affinity binding to HMGB1, namely ODN phosphorothioate backbone and length and, albeit to a lesser extent, base sequence. Finally, we also found that HMGB1, HMGB2, and HMGB3 were all bound directly to ISM ODN (Fig. S1*E*). Collectively, these results are consistent with our previous finding of promiscuous binding of HMGBs (11) and demonstrate that even ni-ODNs can bind HMGBs with high affinity, provided that they have the characteristics defined above.

Suppressive Effect of ISM ODN on Nucleic Acid-Mediated Immune Responses. We next examined whether ISM ODN, which shows the highest binding affinity with HMGBs, suppresses nucleic acid-mediated innate immune responses. As shown in Fig. 2*A*, mouse embryonic fibroblasts (MEFs) pretreated with ISM ODN and subsequently stimulated with poly(dA-dT)·poly(dT-dA) (B-DNA) (19) or poly(I:C) showed markedly suppressed mRNA induction of type I IFNs, IL-6, and RANTES genes compared with mock-treated MEFs; as expected, ISM ODN strongly interferes with the binding of HMGB1 to B-DNA or poly(I:C) (Fig. S2*A*). On the other hand, the mRNA induction of the same genes by lipopolysaccharide (LPS) stimulation remained unaffected (Fig. S2*B*). To examine the correlation between HMGB binding affinity and the suppressive effect of the above ODNs, we compared ISM ODN with CpG-B ODN, ISR ODN, PS, and PD-ISM ODN for their suppressive effect on cytosolic nucleic acid stimulations in MEFs. As shown in Fig. 2*B*, mRNA induction of the cytokine genes was also strongly suppressed by CpG-B or ISR ODNs, albeit less effectively than ISM ODN. On the other hand, the suppressive effect was very weak, if at all, for PS and PD-ISM ODN. Essentially the same observation was made for the induction of IFN-β and IL-6 secretion by ELISA (Fig. S2 *C* and *D*). In addition, A20 or C20 ODNs effectively suppressed IFN-β mRNA induction by B-DNA, whereas the effect diminished rather markedly as ODN length

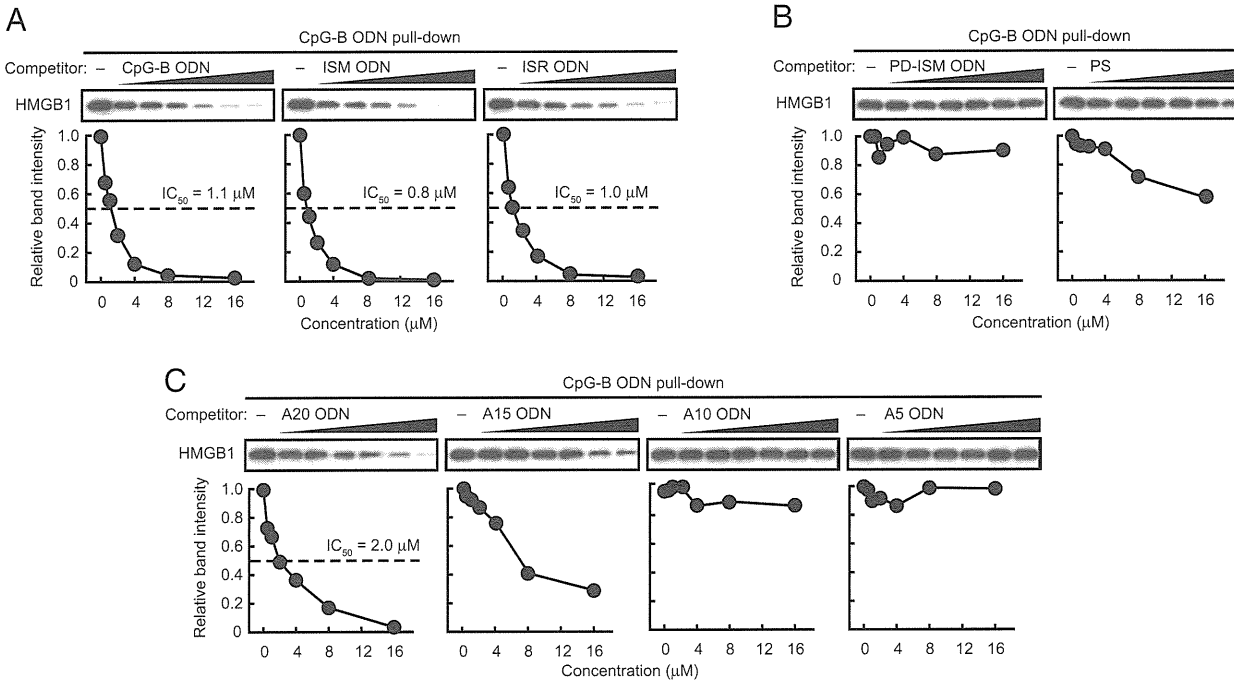

Fig. 1. Binding of HMGB1 to ODNs. Pull-down assay was performed using recombinant HMGB1 and biotin-conjugated CpG-B ODN in the presence of increasing amounts of unconjugated CpG-B, ISM, and ISR ODNs (*A*), PS and PD-ISM ODN (*B*), and A20, A15, A10, and A5 ODNs (*C*) (0.5, 1, 2, 4, 8, or 16 μM). The relative band intensity of precipitated HMGB1 is depicted graphically.

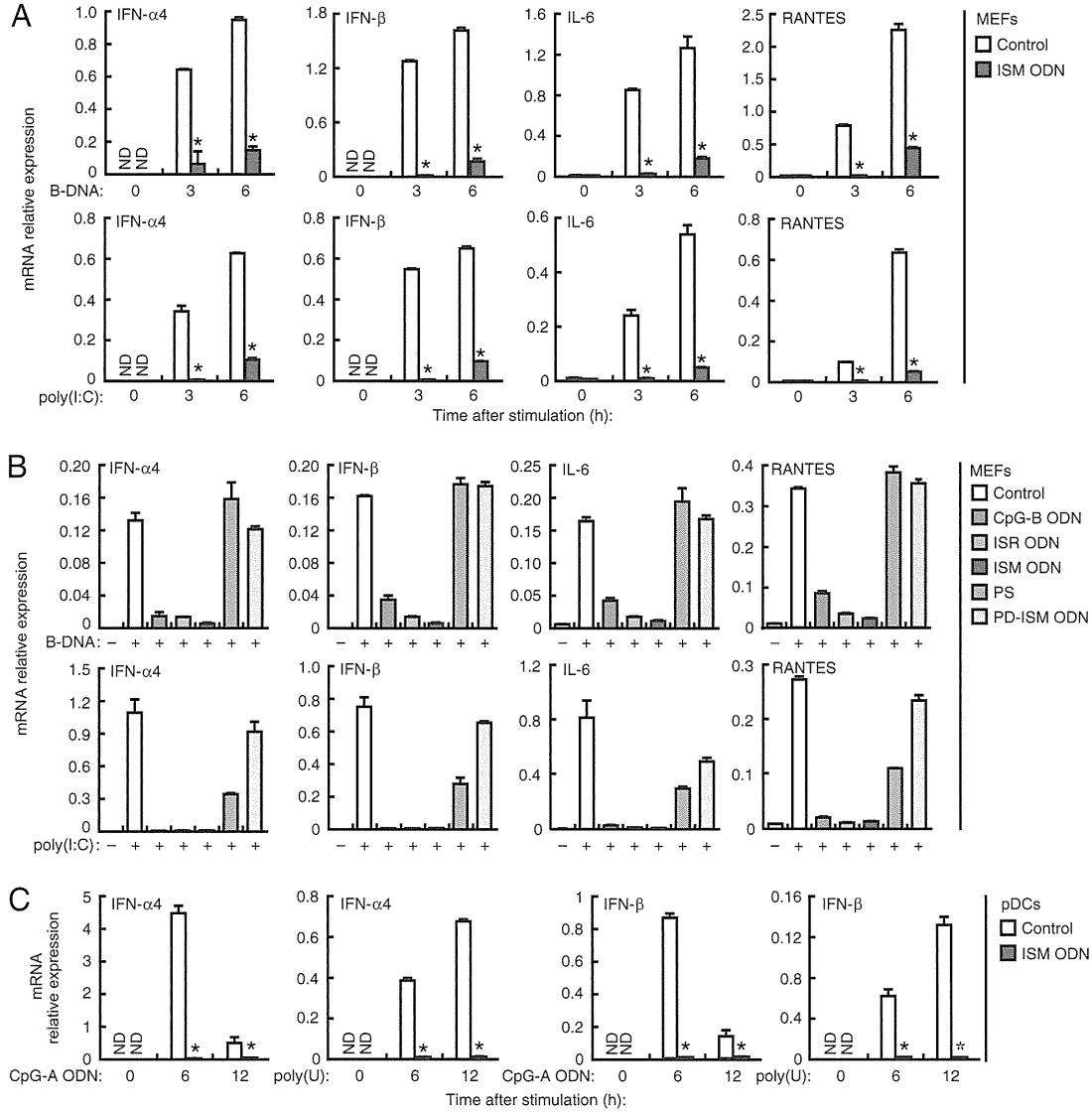

Fig. 2. Suppressive effect of ISM ODN on nucleic acid-mediated innate immune responses. (*A* and *B*) MEFs were left untreated (control) or pretreated with the indicated ODN (1 μM) for 1 h, and then stimulated with B-DNA (5 μg/mL) or poly(I:C) (5 μg/mL) for 3 h (*A* and *B*) or 6 h (*A*). (*C*) Bone marrow-derived pDCs were left untreated (control) or pretreated with ISM ODN for 1 h, and then stimulated with CpG-A ODN (1 μM) or poly(U) (5 μg/mL) for 6 or 12 h. Cytokine mRNA expression levels of the indicated genes were measured by quantitative RT-PCR. $^*P < 0.01$ compared with control. Data in all panels are presented as means and SD ($n = 3$). ND, not detected.

decreased (Fig. S2*E*). Thus, the suppressive effect of each ODN correlates with its binding affinity with HMGB1.

Because HMGBs are essential for both cytosolic and TLR-dependent sensing of nucleic acids (11), we next determined whether TLR responses to nucleic acids are also suppressed by ISM ODN. First, bone marrow cells were cultured in vitro with the Flt3 ligand to enrich plasmacytoid DCs (pDCs), which produce type I IFN en masse upon TLR7 or TLR9 stimulation (20), and the effect of ISM ODN was then examined. As shown in Fig. 2*C*, the mRNA induction by CpG-A ODN or poly(U), which respectively activate TLR9 and TLR7, was strongly suppressed when these cells were pretreated with ISM ODN. Consistent with this, a strong suppression by ISM ODN was also observed on the secretion of IFN-α and IFN-β by these cells (Fig. S2*F*). Similarly, when conventional DCs (cDCs), which were obtained by in vitro culture of bone marrow cells with GM-CSF, were examined for CpG-B ODN-TLR9-mediated IL-6 and TNF-α production, the ISM ODN pretreatment of the cells resulted in a strong suppression, whereas the LPS-TLR4-mediated production of the same cytokines remained unaffected (Fig. S2*G*). Taken together, these findings all support our initial rationalization that ni-ODNs with high affinity for HMGBs can selectively suppress nucleic acid-activated immune responses via cytosolic receptors or TLRs.

Effect of ISM ODN on Cellular Delivery of and Receptor Signaling by Nucleic Acids. To address where these ODNs exert their suppressive effect on nucleic acid-mediated innate immune responses, we first examined whether ISM ODN affects the cellular uptake of B-DNA by fluorescence microscopy. When a macrophage-like cell line, RAW264.7, was pretreated or mock-treated with ISM ODN and then transfected with rhodamine-labeled B-DNA, the B-DNA uptake in the cells was equally observed in the cytosolic fraction as spot-like shapes, suggesting that ISM ODN pretreatment does not interfere with the B-DNA uptake into the cells (Fig. 3*A* and Fig. S3*A*). Similarly, the uptake of CpG-B ODN remained unaffected by ISM ODN pretreatment (Fig. 3*B* and Fig. S3*B*). Interestingly, when rhodamine-conjugated ISM ODN was delivered into the cells, it merged with FITC-labeled dextran, an endosome/lysosome marker, as well as with LysoTracker, a lysosome marker (Fig. S3*C*); this pattern is

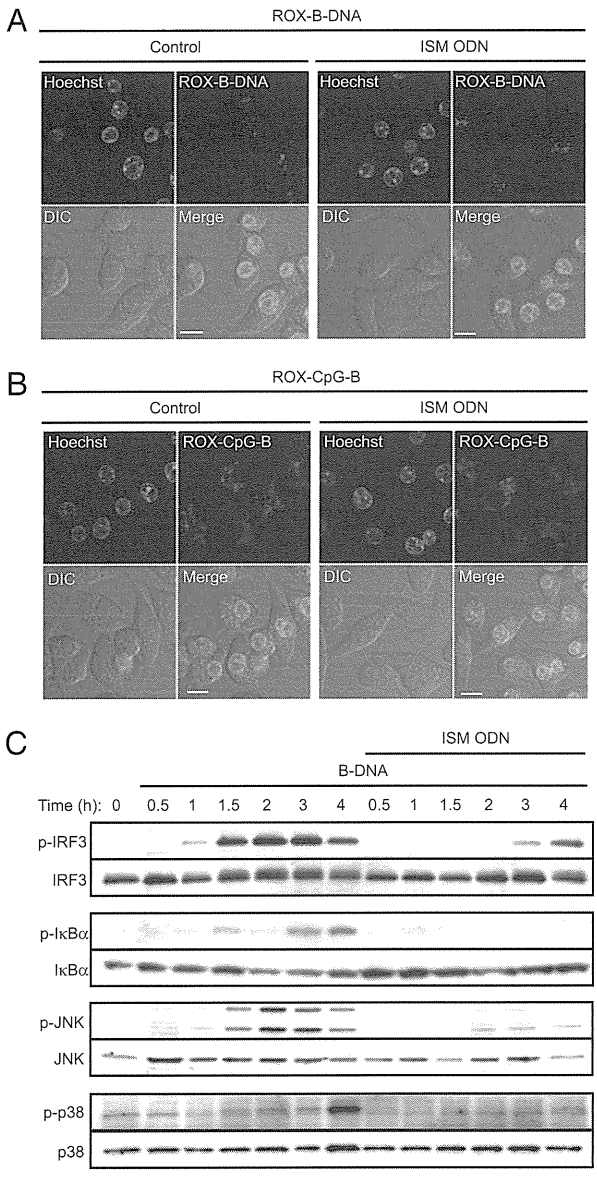

Fig. 3. Suppression of nucleic acid-mediated signaling pathways by ISM ODN. (*A* and *B*) RAW264.7 cells were left untreated (control) (*Left*) or treated with ISM ODN (1 μM) (*Right*) for 1 h, and then stimulated with rhodamine-conjugated B-DNA (1 μg/mL) (ROX-B-DNA; red) (*A*) or rhodamine-conjugated CpG-B ODN (1 μM) (ROX-CpG-B; red) (*B*) for 1 h. Fluorescence images were observed by confocal microscope. The nucleus was stained with Hoechst 33342 (green). (Scale bars, 10 μm.) (*C*) MEFs were left untreated or pretreated with ISM ODN for 1 h, and then stimulated with 10 μg/mL B-DNA for the indicated time periods. The phosphorylation of IRF3, IκB-α, JNK, and p38 was assessed by immunoblot analysis using the indicated antibodies.

essentially similar to that of the TLR9 agonist CpG-B ODN, as demonstrated in previous studies (21, 22), and suggests that the endosomal/lysosomal trafficking of these ODNs occurs similarly. On the other hand, rhodamine-labeled B-DNA merged with dextran but not with LysoTracker (Fig. S3*D*). Thus, taken together with previous reports showing that HMGB1 is also expressed in endosomes (11, 23), these findings suggest that it is the endosomal compartment where ISM ODN exerts its suppressive effect on B-DNA–mediated innate immune signaling by competing with this and other immunogenic nucleic acids for binding with HMGBs (*Discussion*).

To further consolidate the notion that ISM ODN indeed suppresses innate immune signaling, we examined the induction of phosphorylation of IRF3, IκB-α, JNK, and p38 MAPK following cytosolic B-DNA stimulation in MEFs with or without ISM ODN pretreatment. As shown in Fig. 3*C*, the phosphorylation of all was inhibited by ISM ODN pretreatment, which was similarly observed in cells stimulated by poly(I:C) (Fig. S3*E*). Because the sequence of ISM ODN is identical to that of the TLR9 agonist CpG-B ODN aside from one nucleotide, we wished to confirm that the inhibitory effect of ISM ODN is not mediated by TLR9 by any means. When wild-type and *Tlr9*-deficient cDCs were cytosolically stimulated with B-DNA or poly(I:C), we observed that the induction of IL-6 and TNF-α mRNAs was equally suppressed by ISM ODN in cells of both genetic backgrounds, indicating that ISM ODN bound to HMGBs exerts its function independently of TLR9 (Fig. S3*F*). Taken together with these findings, we surmise that ISM ODN does not interfere with the uptake of nucleic acids but rather inhibits the subsequent ligand binding to the PRRs, thereby blocking downstream signal transduction events (*Discussion*).

ISM ODN Suppresses Nucleic Acid-Mediated Immune Responses in Vivo. Nucleic acids potently enhance adaptive immune responses, be they protective or harmful to the host, via the activation of innate immune receptors (24). To investigate the effect of ISM ODN on nucleic acid-mediated adaptive immune responses in vivo, mice were immunized with chicken ovalbumin (OVA) protein using B-DNA or CpG-A ODN as an adjuvant (22) and either with or without pretreatment with ISM ODN, and the induction of $CD8\alpha^+$ cytotoxic T lymphocytes (CTLs) was examined by flow cytometry. As shown in Fig. 4*A*, the induction of OVA-specific CTL responses was strongly suppressed by the pretreatment of mice with ISM ODN. In addition, when OVA-specific IgG1 production was monitored in the sera from mice immunized with OVA and B-DNA, it was found to be suppressed and almost undetectable in ISM ODN-pretreated mice (Fig. S4*A*). Thus, ISM ODN also serves as a potent suppressor of nucleic acid-mediated adaptive immune responses.

Therapeutic Effects of ISM ODN in Immunological Disorder Models. The above findings prompted us to examine whether ISM ODN suppresses inflammation or autoimmune disorders in which the contribution of nucleic acids and/or HMGB1 has been implicated. There is ample evidence that autoantibodies bound to self-DNA or -RNA, or DNA derived from dead cells of inflammatory lesions, can activate nucleic acid-sensing receptors and subsequent immune responses (4, 24–26). A typical example is experimental autoimmune encephalomyelitis (EAE), an animal autoimmune demyelinating disease model of human multiple sclerosis, wherein signaling by nucleic acid-sensing TLRs contributes to the development and pathology of the disease (27–29). Thus, we examined whether ISM ODN can suppress EAE development in mice immunized with myelin oligodendrocyte glycoprotein peptide emulsified in complete Freund's adjuvant. Eight days after immunization, these mice were injected i.v. with ISM ODN or were mock-injected. Remarkably, EAE development, which was observed in the mock-injected mice, was strongly suppressed in the ISM ODN-injected mice (Fig. 4*B*).

We next examined the effect of ISM ODN on an established LPS-induced septic shock model for which an active role for HMGB1 has been reported (30). Interestingly, when mice were i.p. injected with a lethal dose of LPS, those pretreated with ISM ODN showed a significantly high survival rate: As shown in Fig. 4*C*, whereas all mice without ISM ODN pretreatment died within 48 h, 70% of those mice with ODN pretreatment survived even 72 h after LPS injection. It is worth noting that, unlike the control mice, the induction of serum aspartate transaminase (AST) and alanine transaminase (ALT), which are indicators of liver injury, remained strongly suppressed in ISM ODN-pretreated mice 16 h after LPS injection, suggesting that ISM ODN itself has little or no toxicity (Fig. S4*B*). To further examine how ISM ODN suppresses LPS-induced lethality in mice, we analyzed the levels of serum proinflammatory cytokines after LPS injection. As shown in Fig. S4*C*,

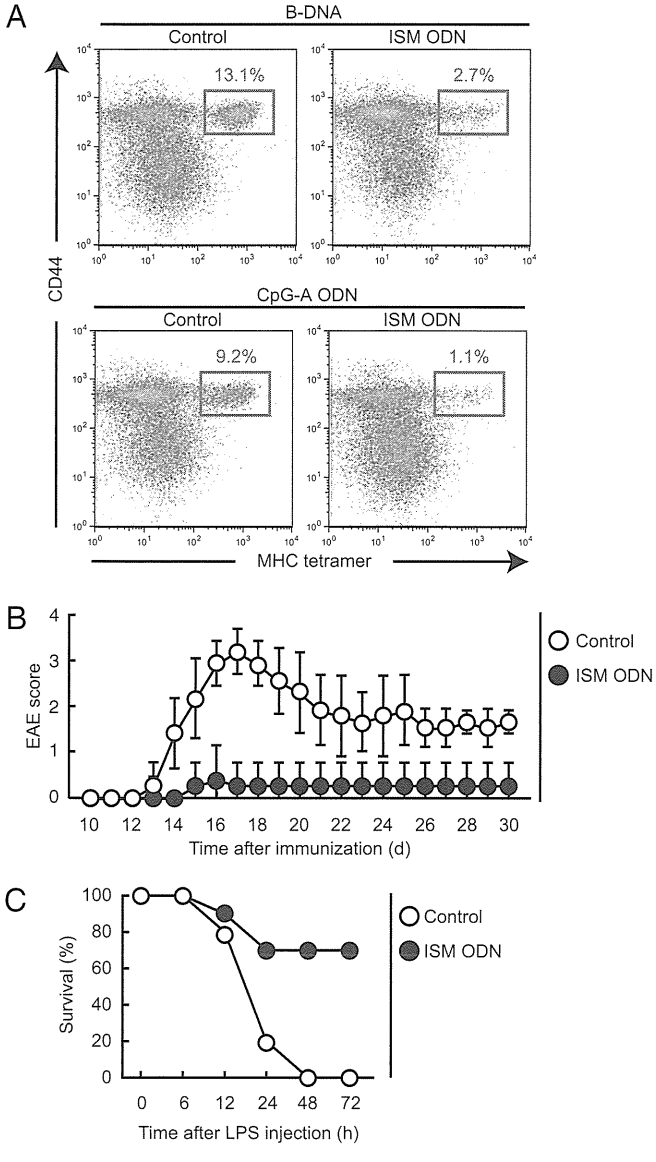

Fig. 4. Effect of ISM ODN on nucleic acid-mediated immune responses and disease models in vivo. (*A*) Mice were immunized with 0.5 mg of OVA and DNA (10 μg of B-DNA or 50 μg of CpG-A ODN) in the presence or absence of 1 mg of ISM ODN. Six days later, splenocytes were isolated and subjected to three-color FACS analysis using an anti-CD8α antibody, anti-CD44 antibody, and OVA-specific MHC class I tetramer. The data shown were gated on CD8α-positive events. The numbers indicate the percentage of tetramer-positive cells relative to the total number of $CD8\alpha^+$ T cells. (*B*) Mean EAE scores ± SD for mice treated with PBS (control) or ISM ODN ($n = 4$ per group) are shown. (*C*) Mice were i.p. injected with 1.25 mg of LPS, with or without (control) 0.1 mg of ISM ODN 1 h before LPS injection. The survival rate of each group was monitored for 72 h ($n = 10$).

IL-6 and TNF-α production levels in sera were found to be the same between ISM ODN-pretreated and mock-pretreated mice 2 h after LPS injection; however, cytokine levels were markedly reduced in the ODN-pretreated mice at later time points. These findings suggest that the early-phase induction of these cytokines via the LPS-TLR4 signaling pathway is not affected by ISM ODN, but rather it is the later-phase induction that is mediated by HMGB1 which is inhibited by the ODN. Indeed, HMGB1 is induced by LPS injection at this later phase (i.e., 8–32 h after injection) (30). It has also been shown that HMGB1, which activates TLR4 and possibly other receptors, is required for a lethal inflammation (12, 13, 16). Thus, these observations raise the interesting possibility that ISM ODN not only suppresses nucleic acid-mediated immune responses but may also affect the activity of HMGB1 as a proinflammatory cytokine (*Discussion*).

Discussion

Nucleic acid-mediated immune responses have become an attractive area of study, given their connection to protective and pathological immunities. In view of our previous finding that HMGBs function as universal sentinels for the innate immune responses activated by nucleic acids (11), we aimed here to demonstrate proof of concept for targeting HMGBs as a means for therapeutic intervention for immunological disorders. To do so, we reasoned that ni-ODNs with a high affinity for HMGBs would interfere with the activation of subsequent nucleic acid-mediated immune responses. Indeed, ISM ODN was found to bind HMGBs with high affinity (Fig. 1 and Figs. S1 *D* and *E* and S2*A*) and to suppress immune responses induced by nucleic acid-sensing cytosolic receptors or TLRs (Fig. 2 and Fig. S2 *C*, *D*, and *F*). Because intracellular uptake/delivery of the immunogenic nucleic acids remained unaffected in the presence of ISM ODN (Fig. 3 *A* and *B*) yet downstream signaling events were suppressed (Fig. 3*C* and Fig. S3*E*), it is likely that ISM ODN competes with immunogenic nucleic acids for HMGB binding. On the basis of our observations (Fig. S3 *C* and *D*) and on previous reports showing that HMGB1 is expressed also in endosomes (11, 23), this suppression of HMGB1 function by ISM ODN likely occurs in endosomal vesicles. This view is consistent with our previous notion that the association of ligands with the endosomal membrane and their binding to innate receptors are the common events for the activation of nucleic acid-mediated immune responses (11, 23, 31).

We surmise further that HMGBs function as essential and common components of nucleic acid ligands, without which nucleic acids cannot efficiently bind and activate their cognate receptors, and that the ni-ODNs described here likely interfere with this critical interaction through their binding to HMGBs. Indeed, our data show a correlation between the binding affinity of ODNs with HMGB1 and the magnitude of the suppressive effect of ODNs. Of the structural elements of ODNs that determine binding affinity with HMGBs, our data indicated that a length of more than 15 nucleotides and a phosphorothioate backbone are most critical (Fig. 1 *B* and *C* and Fig. S1*D*). In this regard, previous reports have shown that one HMGB1 molecule covers 15–18 bp of DNA (32, 33), which corroborates our findings that affinity markedly decreased as the ODNs became shorter than 20 nucleotides (Fig. 1*C* and Fig. S1*D*). Our results also show the importance of phosphorothioate modification of a normal phosphodiester backbone for the high-affinity interaction of ni-ODNs with HMGBs (Fig. 1*B*); it is interesting to note that this backbone structure per se also shows binding affinity with other proteins including TLR9 (18, 34). However, it is clear that the nucleotide bases attached to the backbone are also critical for ODN–HMGB interaction. In an attempt to suppress the activation of TLR7- or TLR9-mediated immune responses, relatively short (15- to 25-mer, in most cases) partially or entirely phosphorothioated ODNs have been studied (35, 36). In addition, several classes of "inhibitory ODNs" have been developed, and some of them are reported to ameliorate disease symptoms of animal models of autoimmune diseases and septic shock (36); however, it has been shown that the affinity of inhibitory ODNs with the receptors does not necessarily correlate with their inhibitory activity (37). In light of our present findings, these ODNs may also exert their inhibitory activities on TLR signaling through their interaction with HMGBs.

Nucleic acid-mediated immune responses have been implicated in the pathogenesis of inflammatory and autoimmune diseases (4, 24). Our present study indicates that ISM ODN may serve as an effective compound for the treatment of autoimmunity and sepsis (Fig. 4 *B* and *C*). Notably, ISM ODN treatment did not affect the growth of primary MEFs in vitro (Fig. S3*G*) and did not change AST and ALT levels in sera (Fig. S4*B*), suggesting that ISM ODN treatment has little, if any, toxic effect. Because it has been sug-

gested that TLR9 signaling is related to the exacerbation of EAE symptoms (28, 29), we surmise that ISM ODN may block pathological TLR9 signaling, thereby attenuating the progression of the disease. Moreover, we show ISM ODN suppression of LPS-mediated endotoxin shock, which provides yet another interesting possibility for ODN-based therapy for sepsis and numerous other inflammatory diseases involving HMGB1 (16). Although further study will be required to clarify how ISM ODN inhibits LPS-mediated endotoxin shock, the following possibilities may be considered. It is possible that ISM ODN inhibits the function of HMGB1 as an inflammatory cytokine when released into the extracellular environment by active secretion from stimulated monocytes/macrophages (30) or by passive diffusion from necrotic cells, functioning as a potent proinflammatory cytokine (12) via the activation of TLR4 and other receptors (13). Thus, ODN interaction with secreted HMGB1 may cause the functional inactivation of HMGB1 as an inflammatory cytokine, possibly through the induction of a conformational change. On the other hand, because ISM ODN shows no effect on LPS-mediated response in vitro (Fig. S2 *B* and *G*), HMGB1 may need to interact with an additional molecule for its inflammatory cytokine action in vivo. Because LPS injection into mice induces massive death of hepatocytes and other cells (38), one possibility is the suppression of inflammatory responses by the necrotic cell-derived DNA that may activate the innate immune receptors via interaction with HMGBs. This notion is supported by our observation that IL-6 and TNF-α production induced by necrotic cells is inhibited by treatment with ISM ODN (Fig. S4*D*). Another intriguing possibility is that HMGB1 secreted from cells associates with nucleic acids and that the resulting complex may be the active form, whose function is inhibited by the ODN.

Because of its inflammatory activity, HMGB1 has been targeted for therapy in the treatment of numerous inflammatory diseases. For instance, a previous study has demonstrated that injection of an anti-HMGB1 antibody protects mice from LPS-induced lethal shock (30). In addition, because the protein is often overexpressed in cancer cells, there is much hope for therapeutic strategies based on targeting HMGB1 (39). Thus, ISM ODN or more effective derivatives may lead to the development of alternate therapeutic interventions for these diseases. Further evaluation of the efficacy and safety of ISM ODN and other ODNs, compared with other strategies targeting HMGB1, will be critical for pursuing such possibilities.

Materials and Methods

Poly(dA-dT)·poly(dT-dA) (B-DNA), poly(U), and LPS were purchased from Sigma. Poly(I:C) was purchased from GE Healthcare Biosciences. ODNs for CpG-B (17), CpG-A (GGtgcatcgatgcaGGGGGg) (40), ISM, ISR, PD-ISM (tccatgaggttcctgatgct), poly(dA), and poly(dC) (uppercase, phosphorothioate backbone; lowercase, phosphodiester backbone) with or without biotin, rhodamine, or FITC were purchased from FASMAC. PS (18) was used as described previously (11). Complex formation of B-DNA, poly(I:C), or poly(U) with Lipofectamine 2000 (Invitrogen) and that of CpG-A ODN with *N*-[1-(2,3-dioleoyloxy)propyl]-*N*, *N*, *N*-trimethylammonium methyl-sulfate (DOTAP) (Roche Applied Science) was prepared as described previously (11, 22). Additional information is available in *SI Materials and Methods*.

ACKNOWLEDGMENTS. This work was supported in part by a Grant-In-Aid for Scientific Research on Innovative Areas and by the Global Center of Excellence Program "Integrative Life Science Based on the Study of Biosignaling Mechanisms" from the Ministry of Education, Culture, Sports, and Science, Japan. T.B. is a research fellow of the Japan Society for the Promotion of Science.

1. Akira S, Uematsu S, Takeuchi O (2006) Pathogen recognition and innate immunity. *Cell* 124:783–801.
2. Medzhitov R (2007) Recognition of microorganisms and activation of the immune response. *Nature* 449:819–826.
3. Pisetsky DS (2008) The role of innate immunity in the induction of autoimmunity. *Autoimmun Rev* 8:69–72.
4. Takeuchi O, Akira S (2010) Pattern recognition receptors and inflammation. *Cell* 140: 805–820.
5. Hemmi H, et al. (2000) A Toll-like receptor recognizes bacterial DNA. *Nature* 408: 740–745.
6. Kawai T, Akira S (2010) The role of pattern-recognition receptors in innate immunity: Update on Toll-like receptors. *Nat Immunol* 11:373–384.
7. Yoneyama M, et al. (2005) Shared and unique functions of the DExD/H-box helicases RIG-I, MDA5, and LGP2 in antiviral innate immunity. *J Immunol* 175:2851–2858.
8. Choi MK, et al. (2009) A selective contribution of the RIG-I-like receptor pathway to type I interferon responses activated by cytosolic DNA. *Proc Natl Acad Sci USA* 106: 17870–17875.
9. Takaoka A, et al. (2007) DAI (DLM-1/ZBP1) is a cytosolic DNA sensor and an activator of innate immune response. *Nature* 448:501–505.
10. Schroder K, Muruve DA, Tschopp J (2009) Innate immunity: Cytoplasmic DNA sensing by the AIM2 inflammasome. *Curr Biol* 19:R262–R265.
11. Yanai H, et al. (2009) HMGB proteins function as universal sentinels for nucleic-acid-mediated innate immune responses. *Nature* 462:99–103.
12. Scaffidi P, Misteli T, Bianchi ME (2002) Release of chromatin protein HMGB1 by necrotic cells triggers inflammation. *Nature* 418:191–195.
13. Bianchi ME (2009) HMGB1 loves company. *J Leukoc Biol* 86:573–576.
14. Sims GP, Rowe DC, Rietdijk ST, Herbst R, Coyle AJ (2010) HMGB1 and RAGE in inflammation and cancer. *Annu Rev Immunol* 28:367–388.
15. Apetoh L, et al. (2007) The interaction between HMGB1 and TLR4 dictates the outcome of anticancer chemotherapy and radiotherapy. *Immunol Rev* 220:47–59.
16. Andersson U, Tracey KJ (2011) HMGB1 is a therapeutic target for sterile inflammation and infection. *Annu Rev Immunol* 29:139–162.
17. Krieg AM, et al. (1995) CpG motifs in bacterial DNA trigger direct B-cell activation. *Nature* 374:546–549.
18. Haas T, et al. (2008) The DNA sugar backbone 2′ deoxyribose determines Toll-like receptor 9 activation. *Immunity* 28:315–323.
19. Ishii KJ, et al. (2006) A Toll-like receptor-independent antiviral response induced by double-stranded B-form DNA. *Nat Immunol* 7:40–48.
20. Colonna M, Trinchieri G, Liu YJ (2004) Plasmacytoid dendritic cells in immunity. *Nat Immunol* 5:1219–1226.
21. Latz E, et al. (2004) TLR9 signals after translocating from the ER to CpG DNA in the lysosome. *Nat Immunol* 5:190–198.
22. Honda K, et al. (2005) IRF-7 is the master regulator of type-I interferon-dependent immune responses. *Nature* 434:772–777.
23. Ivanov S, et al. (2007) A novel role for HMGB1 in TLR9-mediated inflammatory responses to CpG-DNA. *Blood* 110:1970–1981.
24. Iwasaki A, Medzhitov R (2010) Regulation of adaptive immunity by the innate immune system. *Science* 327:291–295.
25. Lövgren T, Eloranta ML, Båve U, Alm GV, Rönnblom L (2004) Induction of interferon-α production in plasmacytoid dendritic cells by immune complexes containing nucleic acid released by necrotic or late apoptotic cells and lupus IgG. *Arthritis Rheum* 50: 1861–1872.
26. Marshak-Rothstein A, Rifkin IR (2007) Immunologically active autoantigens: The role of Toll-like receptors in the development of chronic inflammatory disease. *Annu Rev Immunol* 25:419–441.
27. Marta M, Andersson A, Isaksson M, Kämpe O, Lobell A (2008) Unexpected regulatory roles of TLR4 and TLR9 in experimental autoimmune encephalomyelitis. *Eur J Immunol* 38:565–575.
28. Prinz M, et al. (2006) Innate immunity mediated by TLR9 modulates pathogenicity in an animal model of multiple sclerosis. *J Clin Invest* 116:456–464.
29. Segal BM, Chang JT, Shevach EM (2000) CpG oligonucleotides are potent adjuvants for the activation of autoreactive encephalitogenic T cells in vivo. *J Immunol* 164: 5683–5688.
30. Wang H, et al. (1999) HMG-1 as a late mediator of endotoxin lethality in mice. *Science* 285:248–251.
31. Tian J, et al. (2007) Toll-like receptor 9-dependent activation by DNA-containing immune complexes is mediated by HMGB1 and RAGE. *Nat Immunol* 8:487–496.
32. Saito K, Kikuchi T, Shirakawa H, Yoshida M (1999) The stabilized structural array of two HMG1/2-boxes endowed by a linker sequence between them is requisite for the effective binding of HMG1 with DNA. *J Biochem* 125:399–405.
33. Stott K, Tang GS, Lee KB, Thomas JO (2006) Structure of a complex of tandem HMG boxes and DNA. *J Mol Biol* 360:90–104.
34. Peck ML, Herschlag D (1999) Effects of oligonucleotide length and atomic composition on stimulation of the ATPase activity of translation initiation factor eIF4A. *RNA* 5:1210–1221.
35. Halpern MD, Pisetsky DS (1995) In vitro inhibition of murine IFN γ production by phosphorothioate deoxyguanosine oligomers. *Immunopharmacology* 29:47–52.
36. Lenert PS (2010) Classification, mechanisms of action, and therapeutic applications of inhibitory oligonucleotides for Toll-like receptors (TLR) 7 and 9. *Mediators Inflamm* 2010:986596.
37. Ashman RF, Goeken JA, Latz E, Lenert P (2011) Optimal oligonucleotide sequences for TLR9 inhibitory activity in human cells: Lack of correlation with TLR9 binding. *Int Immunol* 23:203–214.
38. Nolan JP (1981) Endotoxin, reticuloendothelial function, and liver injury. *Hepatology* 1:458–465.
39. Tang D, Kang R, Zeh HJ, III, Lotze MT (2010) High-mobility group box 1 and cancer. *Biochim Biophys Acta* 1799:131–140.
40. Verthelyi D, Ishii KJ, Gursel M, Takeshita F, Klinman DM (2001) Human peripheral blood cells differentially recognize and respond to two distinct CPG motifs. *J Immunol* 166:2372–2377.

EXPERIMENTAL CELL RESEARCH 317 (2011) 221–233

available at www.sciencedirect.com

ScienceDirect

www.elsevier.com/locate/yexcr

Research Article

Community effect triggers terminal differentiation of myogenic cells derived from muscle satellite cells by quenching Smad signaling

Michiko Yanagisawa[a,b,1], *Atsushi Mukai*[a,1], *Kosuke Shiomi*[a], *Si-Yong Song*[c], *Naohiro Hashimoto*[a,*]

[a]*Department of Regenerative Medicine, National Institute for Longevity Sciences, National Center for Geriatrics and Gerontology, 35 Gengo, Morioka, Oobu, Aichi 474-8522, Japan*

[b]*Aging Research, Nagoya University Graduate School of Medicine, 65 Tsurumai-cho, Showa-ku, Nagoya, Aichi 466-8550, Japan*

[c]*Institute of Neuroscience, Faculty of Pharmaceutical Sciences at Kagawa, Tokushima Bunri University, 1314-1 Shido, Sanuki-shi, Kagawa 769-2193, Japan*

ARTICLE INFORMATION

Article Chronology:
Received 18 April 2010
Revised version received
16 September 2010
Accepted 13 October 2010
Available online 20 October 2010

Keywords:
Community effect
BMP
Smad
ALK
Myogenesis
Osteogenesis

ABSTRACT

A high concentration of bone morphogenetic proteins (BMPs) stimulates myogenic progenitor cells to undergo heterotopic osteogenic differentiation. However, the physiological role of the Smad signaling pathway during terminal muscle differentiation has not been resolved. We report here that Smad1/5/8 was phosphorylated and activated in undifferentiated growing mouse myogenic progenitor Ric10 cells without exposure to any exogenous BMPs. The amount of phosphorylated Smad1/5/8 was severely reduced during precocious myogenic differentiation under the high cell density culture condition even in growth medium supplemented with a high concentration of serum. Inhibition of the Smad signaling pathway by dorsomorphin, an inhibitor of Smad activation, or noggin, a specific antagonist of BMP, induced precocious terminal differentiation of myogenic progenitor cells in a cell density-dependent fashion even in growth medium. In addition, Smad1/5/8 was transiently activated in proliferating myogenic progenitor cells during muscle regeneration in rats. The present results indicate that the Smad signaling pathway is involved in a critical switch between growth and differentiation of myogenic progenitor cells both in vitro and in vivo. Furthermore, precocious cell density-dependent myogenic differentiation suggests that a community effect triggers the terminal muscle differentiation of myogenic cells by quenching the Smad signaling.

Introduction

Signaling molecules have both permissive and repressive effects on gene expression in the myotomes during embryonic myogenesis. Skeletal muscle formation in the paraxial mesoderm is controlled by a number of signaling molecules emanating from neighboring tissues. Sonic hedgehog (Shh) and Wnt promote myogenesis [1]. In contrast, bone morphogenetic protein 4 (BMP4) inhibits premature differen-

* *Corresponding author.* Fax: +81 562 46 8464.
E-mail address: nao@ncgg.go.jp (N. Hashimoto).

Abbreviations: BMP, bone morphogenetic protein; ALK, activin-like kinase; MyHC, myosin heavy chain; BPV, bupivacaine hydrochloride

[1] These authors equally contributed to this study.

0014-4827/$ – see front matter © 2010 Elsevier Inc. All rights reserved.
doi:10.1016/j.yexcr.2010.10.011

tiation of the paraxial mesoderm. In addition, the negative action of BMP4 is counteracted by a specific BMP antagonist, noggin [1].

In contrast to embryonic skeletal muscle formation, the contribution of the signaling molecules to regulation of myogenesis during postnatal growth and repair of skeletal muscles remains to be determined. Skeletal muscle stem cells of adult muscle are known as muscle satellite cells that were characterized as a different class of myogenic cells from embryonic and fetal myoblasts [2]. Nonetheless, the signaling molecules that control embryonic and fetal myogenesis are likely to play a role in the regulation of growth and differentiation of muscle satellite cells and their descendant progenitor cells. Shh and Wnt have been reported to promote the proliferation of postnatal myogenic cells derived from muscle satellite cells [3–6]. It has been well established that BMPs induce heterotopic osteogenic terminal differentiation in myogenic cells derived from satellite cells [7–9]. Forced expression of constitutively active forms of BMP type I receptors and those of activin-like kinases (ALK) or receptor-regulated Smads (Smad1/5/8) induces ectopic osteogenesis in myogenic cells [10–13]. These results strongly suggest that the BMP–ALK–Smad signaling pathway renders the myogenic cell fate osteogenic. However, the concentration of exogenous BMPs required to induce osteogenesis in more than a half of myogenic cells is 100 ng/ml or higher [8,9,14,15] (Supplementary Fig. S1; Hashimoto, unpublished data). Recently, gene expression analyses of human skeletal muscle demonstrate that BMP4 is involved in the regulation of myogenic progenitor proliferation in human fetal skeletal muscle [16]. Co-Smad, Smad4, is involved in the inhibition of myogenesis but not the induction of osteogenesis, both of which are triggered by BMPs [15]. Therefore, these studies imply that the Smad signaling pathway plays a distinct role independently of heterotopic osteogenesis.

In vitro culture systems of myogenic cells have greatly contributed to elucidation of the molecular mechanisms underlying myogenic terminal differentiation of muscle satellite cells. Mouse and rat myoblast cell lines such as C2C12 [17], Ric10 [18], and L6 [19] from muscle satellite cells in postnatal muscle have been established and represent excellent cell culture models to analyze the proliferation and differentiation of myogenic progenitor cells. Terminal muscle differentiation of myoblastic cells is usually induced by reduction of the serum concentration in the culture medium. A number of studies have provided mechanistic insights into myogenesis using this differentiation-inducing condition because terminal muscle differentiation is synchronously induced in cells cultured in the serum-reduced differentiation medium. Nevertheless, we should keep in mind that the reduction of serum and/or growth factors would never be triggering mechanisms of terminal muscle differentiation in vivo. Another option to induce myogenesis of cultured myoblasts is high cell density culture. A number of muscle cell biologists may have had the common experience of myogenic cells beginning to undergo terminal muscle differentiation even in growth medium supplemented with a high concentration of serum when cultures become confluent. The spontaneous differentiation occurs asynchronously and focally in myoblast cultures under that growth condition. Thus, cell density-dependent and growth factor-independent induction of spontaneous myogenesis in vitro might be a unique model to investigate the initiation of myogenesis in regenerating muscles, which may contain large amounts of growth factors and cytokines. Mechanistic insights into spontaneous myogenesis may provide a new hypothesis concerning the molecular switch between growth and differentiation of myogenic cells during muscle regeneration.

In this study, we focused on the physiological role of the Smad signaling pathway in the switch between growth and differentiation of myogenic progenitor cells. Smad1/5/8 was activated in undifferentiated mouse myogenic Ric10 cells under growth conditions without the stimulus of exogenous BMPs. We show here that the community effect of myogenic cells quenches the Smad signaling pathway and triggers terminal muscle differentiation.

Materials and methods

Cell culture

The mouse myogenic cell line Ric10 was established from muscle satellite cells of the normal gastrocnemius muscle of an adult female ICR mouse [9,18,20]. Ric10 cells were plated on dishes coated with type I collagen (Sumilon, Tokyo, Japan) and cultured at 37 °C under 10% CO_2 in primary myocyte growth medium (pmGM) consisting of Dulbecco's modified Eagle's medium supplemented with 20% fetal bovine serum (FBS), 2% Ultroser G (Biosepra, Cedex-Saint-Christophe, France), and glucose (4.5 mg/ml) [9,14,21,22]. For induction of myogenic differentiation, the cells were plated and cultured for 24 h in pmGM, and then the medium was changed to primary myocyte differentiation medium (pmDM) consisting of the chemically defined medium TIS [23,24] supplemented with 2% FBS.

For micromass culture, dissociated single cells were cultured in pmGM at a density of 5×10^4 or 1×10^5 cells per 100-μl spot in a 35-mm dish or 5×10^2–2.5×10^4 cells per 50-μl spot in a well of a 24-well plate. After incubation for at least 2 h, pmGM was carefully added to each dish or well.

For inhibition of the Smad signaling pathway, Ric10 cells were cultured in medium supplemented with dorsomorphin (Calbiochem, Darmstadt, Germany) or recombinant mouse noggin and Fc of human IgG_1 chimeric protein (R&D Systems, Minneapolis, MN).

Promoter assay

Ric10 cells (2×10^4 per well in 12-well plates) were transfected with 0.75 μg of plasmids in the presence of 4.5 μl of FuGENE6 transfection reagent (Roche Diagnostic, Mannheim, Germany) as described [20,23–25]. A reporter plasmid MGN-luc was constructed by subcloning a 1.4 kb fragment of mouse myogenin promoter [26] (kindly provided by Y. Nabeshima) into pGL2 (Promega, Madison, WI). The transcriptional activity of Smad1/5/8 was determined using a BMP/Smad-dependent specific enhancer-containing reporter plasmid BRE-luc [27] (kindly provided by K. Miyazono). FLAG-tagged mouse Smad6 cDNA (kindly provided by K. Watanabe) and ALK2(KR) cDNA encoding a dominant negative form of human ALK2 (kindly provided by T. Imamura) were subcloned into pcDNA3 (Invitrogen, San Diego, CA). An expression plasmid for *Renilla* luciferase, pRL-TK (Promega) was co-transfected for normalization of transfection efficiency. A dual luciferase assay using a dual luciferase assay system was done essentially according to the manufacturer's instructions (Promega).

Induction of muscle regeneration by bupivacaine

Gastrocnemius muscles of Sprague–Dawley rats were injected with 500 μl of 0.5% bupivacaine hydrochloride (Marcain; Astellas Pharma, Tokyo, Japan) [28]. Three to four days after injection, the

gastrocnemius muscles were removed and quickly frozen in isopentane cooled with liquid nitrogen and processed for preparation of cryosections as described [29]. Muscle specimens were sectioned at a thickness of 8 μm with a cryostat.

Immunofluorescence analysis

The frozen sections and cultured cells were fixed with 4% paraformaldehyde for 10 min at room temperature or on ice, respectively, and then incubated with primary antibodies. Primary antibodies included mouse monoclonal antibodies to mouse MyoD (1:10, Novocastra, Newcastle, UK), chicken sarcomeric myosin heavy chain (MHyC) (MF20, undiluted culture supernatant) [30], rat myogenin [31] (ascites, 1:1000, Developmental Studies Hybridoma Bank, Iowa City, IA), rabbit polyclonal antibodies to human phosphorylated Smad1/5/8 (pSmad) (1:100, Cell Signaling, Denver, CO), rat myogenin (1:200) [25], or mouse Id1 (1:100, affinity purified antibodies against β-galactosidase-mouse Id1 fusion protein) (Hashimoto, unpublished). Secondary antibodies included biotinylated or Cy3-labeled antibodies to mouse or rabbit immunoglobulin G (Jackson ImmunoResearch Laboratory, Bar Harbor, ME). The biotinylated antibodies were detected with streptavidin-conjugated Alexa488 (Jackson ImmunoResearch Laboratory). Cell nuclei were stained with 2,4-diamidino-2-phenylindole dihydrochloride n-hydrate (DAPI) (Sigma, St. Louis, MO). Samples were visualized using an upright microscope (model BX50; Olympus, Tokyo, Japan) and an inverted microscope (model IX71; Olympus) and a CCD camera (DP70; Olympus). Images were post processed using Adobe Photoshop (Adobe Systems, San Jose, CA). The signal intensity of pSmad in the nucleus was quantified using Image J software (NIH, Bethesda, MA). The signal density of pSmad in each sample was estimated from [signal intensity/nuclear area].

Immunoblotting

Sample preparation and immunoblot analysis were performed as described [24,25,32]. Immune complexes were detected by colorimetry with a BCIP/NBT detection kit (Nacalai, Kyoto, Japan) or an ECL kit (GE Healthcare, Piscataway, NJ). Primary antibodies included antibodies to MyHC, myogenin, Smad1 (Abcam, Cambridge, MA), pSmad, Id1 (Santa Cruz Biotech., Santa Cruz, CA) and flotilin-1 (Santa Cruz Biotech). Secondary antibodies included alkaline phosphatase (DAKO, Carpinteria, CA)- or horseradish peroxidase (GE Healthcare)-labeled antibodies to mouse or rabbit immunoglobulin G. The PVDF membranes (Fluoro Trans W; Pall, Port Washington, NY) or X-ray films (Hyperfilm ECL; GE Healthcare) were scanned, and the signal intensity of each band was quantified using Image J software.

Results

Smad1/5/8 are phosphorylated in undifferentiated myogenic cells under growth conditions

To understand the physiological role of BMP–ALK–Smad signaling pathway during the growth and differentiation of postnatal myogenic cells, we detected phosphorylated Smad1/5/8 in the mouse myogenic progenitor cell line Ric10 with or without BMP2 stimulation. Smad1, Smad5, and Smad8 are functionally activated through their phosphorylation in a BMP–ALK–Smad axis-dependent manner [33]. The amount of Smad1, a major Smad protein in Ric10 cells, remained constant even under BMP stimulation (Fig. 1A, upper panel). Exogenous BMP2 activated the Smad signaling pathway: although the amount of phosphorylated Smad1/5/8 in BMP-stimulated Ric10 cells was not more than 1.5 times that in unstimulated cells (Fig. 1A), exogenous BMP2 multiplied the transcriptional activity of Smad1/5/8 up to more than 10 times that in unstimulated cells (Fig. 1Ba). However, Smad1/5/8 was also phosphorylated in growing Ric10 cells without exposure to any exogenous ligand (Fig. 1A, left lane). Phosphorylated Smad1/5/8 was localized in nuclei of unstimulated, growing Ric10 cells (Fig. 1C). In addition, ALK2(KR), the dominant negative form of ALK2, significantly reduced the transcriptional activity of Smad1/5/8 in unstimulated cells (Fig. 1Bb). Exogenous BMP2 induced glycosylphosphatidylinositol-anchored alkaline phosphatase (ALP), an early marker of osteogenic differentiation through the activation of Smad signaling pathway in mouse myogenic cells (Supplementary Fig. S1) [9,14]. In contrast, the basal level activation of Smad1/5/8 didn't induce ALP expression in unstimulated mouse myogenic cells (data not shown) [9,14]. The results suggest that the Smad signaling pathway plays a physiological role that is independent of osteogenic differentiation in unstimulated, undifferentiated growing Ric10 cells.

Myogenic terminal differentiation-inducing conditions reduce the amount of phosphorylated Smad1/5/8

Myogenic terminal differentiation of cultured myogenic cells depends highly on both the serum concentration in the medium and the cell density in the culture. Despite the low cell density, myogenic progenitor cells actually undergo myogenic differentiation in differentiation medium supplemented with a low concentration of serum. However, myogenic cells under the high cell density culture condition give rise to myotubes faster than those under the low cell density

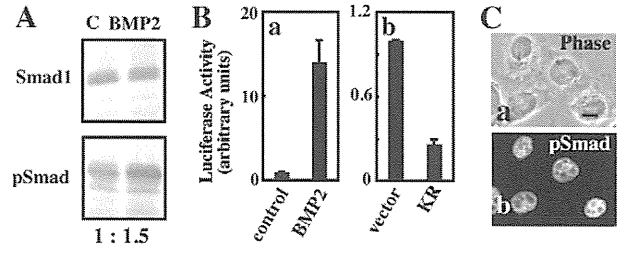

Fig. 1 – Phosphorylation of Smad1/5/8 in undifferentiated growing myogenic cells. (A) Total protein (20 mg) was prepared from Ric10 cells that had been cultured in pmGM supplemented with (lane BMP2) or without (lane C) BMP2 (100 ng/ml) for 24 h. Smad1 and phosphorylated Smad1/5/8 (pSmad) were detected on immunoblots. Relative amounts of pSmad are shown below the lower panel. (B) Ric10 cells were transfected with BRE-luc, Renilla luciferase-expression plasmid pRL-tk, and pcDNA3.1 (a and vector in b) or an expression plasmid for dominant negative ALK2 (KR). Then the cells were cultured in pmDM for 24 h and harvested for dual luciferase assay according to the manufacturer's instructions (Hashimoto and Ogashiwa, 1997). In (a), the cells were stimulated with BMP2 (100 ng/ml) or without (control) for 24 h. (C) Unstimulated, growing Ric10 cells showed nuclear localization of pSmad. The images were obtained by phase contrast (a) and epifluorescent (b) microscopy. Scale bar: 10 μm.

culture condition. To reveal the optimal culture condition for myogenic differentiation, different numbers of Ric10 cells were cultured for 24 h in the chemically defined differentiation medium TIS supplemented with different concentrations of serum. Actually, myogenic differentiation of Ric10 cells was exclusively induced under the culture condition with low serum and high cell density in an early period of culture (Fig. 2A). Then we determined the activation level of the Smad signaling pathway in Ric10 cells under different culture conditions. Smad1/5/8 was phosphorylated in low cell density culture (Fig. 2B, lower panel). In contrast, the amount of phosphorylated Smad1/5/8 severely declined in the high cell density culture. The serum concentration in the medium also affected the phosphorylation level of Smad1/5/8 both in low and high cell density cultures. In addition, a low cell density in the culture and a high serum concentration in the medium synergistically activated the Smad signaling pathway (Fig. 2C). However, a low cell density in the culture more potently activated the Smad signaling pathway than a high serum concentration in the medium.

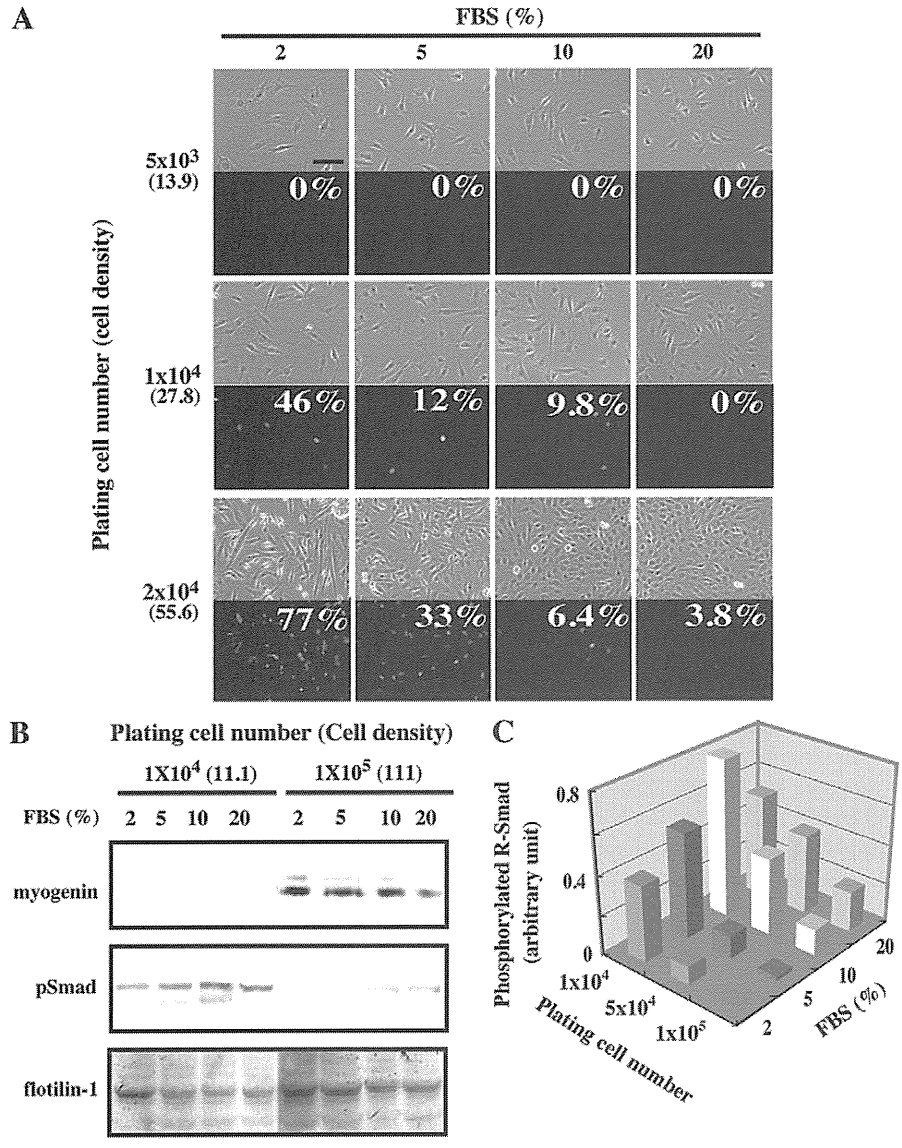

Fig. 2 – Down-regulation of Smad signaling pathway under myogenic differentiation-inducing conditions. (A) **Ric10 cells were plated at a density of 5×10^3, 1×10^4, and 2×10^4 cells in a well of a 12-well culture plate and then cultured for 24 h in medium supplemented with different concentrations of fetal bovine serum (FBS). Cell density at seeding (cells per mm^2) is shown in parentheses left of the panels. Myogenin-positive nuclei were detected with a specific antibody and appeared as green dots. The percentage of myogenin-positive nuclei is shown inside the panels. Phase contrast and immunofluorescence images of the identical fields are shown as pairs. Scale bar: 100 μm. (B and C) Different numbers of Ric10 cells were plated in 35-mm dishes and cultured for 24 h in medium supplemented with different concentrations of FBS. Cell density at seeding (cells per mm^2) is shown in parentheses in (B). Myogenin, pSmad, and flotilin-1 were detected in 20 mg of total protein by immunoblotting analysis. Flotilin-1 was used as a loading control. Amounts of phosphorylated Smad1/5/8 on immunoblots were quantified and are represented as a three-dimensional graph (C).**

The myogenic differentiation-specific transcription factor myogenin was expressed exclusively in the high cell density cultures of Ric10 cells, in which phosphorylation of Smad1/5/8 was down-regulated (Fig. 2B, upper panel). It should be noted that Ric10 cells undergo myogenic differentiation during prolonged culture (more than 48 h), even under the low cell density culture condition (Fig. 3A) [18]. Therefore, myogenic terminal differentiation was enhanced in the high cell density culture associated with inactivation of the Smad signaling pathway. The results suggest that the Smad signaling pathway is activated in undifferentiated proliferating cells and inactivated during the myogenic differentiation induced under the high cell density culture condition. The results imply the involvement of the Smad signaling pathway in a critical switch between growth and differentiation of myogenic cells.

Quenching of Smad signaling pathway is rate-limiting for myogenic differentiation induced by serum reduction

To determine whether the Smad signaling pathway is involved in the regulation of myogenic differentiation triggered by serum reduction, Ric10 cells were seeded at low (22 cells per mm^2) or high (111 cells per mm^2) cell density and then induced to differentiate in differentiation medium pmDM containing 2% serum for up to 48 h. Ric10 cells seeded at high cell density gave rise to myotubes after 24 h under the serum-reduced culture condition whereas those under the low cell density culture condition began to fuse after 36 h (Fig. 3A). Expression of myogenin and a muscle differentiation marker MyHC was induced by serum reduction faster in the high cell density culture than the low cell density culture (Fig. 3B). In contrast to the muscle-specific proteins, the amount of a downstream factor of the Smad signaling pathway, Id1, declined faster in the high cell density culture than the low cell density culture. Serum reduction decreased the amount of phosphorylated Smad1/5/8 in both low and high cell density cultures. However, the phosphorylated Smad1/5/8 still remained under the serum-reduced, low cell density culture condition (Fig. 3B).

The previously mentioned results imply that quenching of the Smad signaling pathway is rate-limiting for myogenic differentiation induced by serum reduction. To explore this possibility, Ric10 cells were treated with the Smad signaling pathway inhibitor dorsomorphin [34]. Ric10 cells were seeded at low cell density (18 cells per mm^2) and then induced to differentiate in pmDM for up to 48 h. More than 90% of Ric10 cells underwent myogenic differentiation under this condition (Fig. 3A) [18]. Dorsomorphin further reduced the amount of remaining

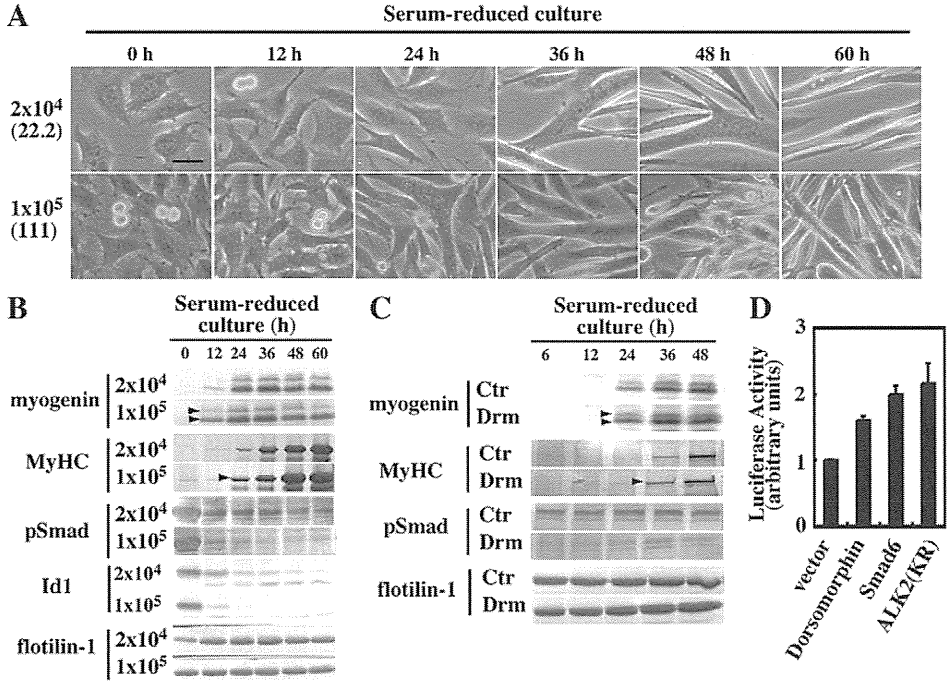

Fig. 3 – Activation levels of Smad signaling pathway during serum-reduced, low cell density culture. (A and B) Ric10 cells (2×10^4 cells per 35-mm dish; 22 cells per mm^2 for low cell density culture or 1×10^5 per 35-mm dish; 111 cells per mm^2 for high cell density culture) were plated and cultured in pmDM for up to 60 h. Images in (A) were obtained by phase contrast microscopy. Scale bar: 50 μm. Total cell lysates (20 μg of proteins) were subjected to immunoblotting analyses for MyHC, myogenin, pSmad, Id1, and flotilin-1 (B). Flotilin-1 was used as a loading control. Plating cell number is shown at the left of panels. Cell density at seeding (cells per mm^2) is shown in parentheses in (B). Arrowheads indicate the enhanced expression of MyHC and myogenin. (C) Ric10 cells (1×10^5 per 100-mm dish; 18 cells per mm^2) were cultured in pmDM with dorsomorphin (3 μM) or without (Control) for the indicated periods (h) shown at the top of panels. Total cell lysates (20 μg of proteins) were subjected to immunoblotting analyses for MyHC, myogenin, pSmad, and flotilin-1. Flotilin-1 was used as a loading control. Arrowheads indicate the enhanced expression of MyHC and myogenin in dorsomorphin-treated culture. (D) Ric10 cells were transfected with MGN-luc, pRL-tk, and pcDNA3.1 (vector and Dorsomorphin) or an expression plasmid for Smad6 or dominant negative ALK2 (ALK2(KR)). Then the cells were cultured in pmDM for 24 h and harvested for dual luciferase assay.

phosphorylated Smad1/5/8 (Fig. 3C). Expression of myogenin and MyHC was enhanced in Ric10 cells treated with dorsomorphin at 24 and 36 h of culture in pmDM. Taken together with the results, lowering the level of phosphorylated Smad may enhance myogenic differentiation triggered by serum reduction.

To determine whether the myogenic differentiation is negatively regulated through the activation of Smad1/5/8 under the serum-reduced culture condition, we determined the promoter activity of myogenin in Ric10 cells when the function of Smad1/5/8 was directly inhibited at distinct steps of the cellular signaling pathway: dorsomorphin inhibits phosphorylation of Smad1/5/8. Smad6, an inhibitory Smad, interrupts the interaction between Smad1/5/8 and Smad4 or BMP type I receptors [35,36]. ALK2(KR), the dominant negative form of ALK2, suppresses the activation of the BMP-receptor ALK2 [12]. Activity of the myogenin promoter in Ric10 cells during 24 h of differentiation culture was significantly enhanced by administration of dorsomorphin or expression of Smad6 or ALK2 (KR) (Fig. 3D). The results suggest that the quenching of Smad signaling pathway plays a role in the rate-determining step of terminal muscle differentiation triggered by serum reduction.

Concentration of phosphorylated Smad1/5/8 declines during myogenic differentiation in a cell density-dependent fashion

High cell density culture is another option for induction of myogenic differentiation in vitro. Ric10 cells were cultured in micromass to undergo myogenic differentiation independently of the serum concentration in the medium. When 5×10^4 or 1×10^5 Ric10 cells were seeded in a 100-μl spot, cells gave rise to a circular mass, the diameter of which was 6–8 mm (Fig. 4A). The cell density within a micromass declined along a central–peripheral axis. Myogenic terminal differentiation was induced exclusively in the central region of a cell mass during the 48 h after seeding, even when cells were cultured in growth medium pmGM containing 20% serum and supplementary growth factors (Fig. 4B). In the central region of the culture, the extremely high cell density was associated with a loss of phosphorylated Smad1/5/8 and the induction of myogenin expression even in pmGM (Fig. 4C). Myogenin expression was induced in a fraction of the nuclei in which the amount of phosphorylated Smad1/5/8 was severely reduced (Supplementary Fig. S2). In contrast, the cells retained phosphorylated Smad1/5/8 and did not express myogenin in the peripheral region with relatively low cell density. The results indicate that the Smad signaling pathway was inactivated under the high cell density culture condition, and also suggest that quenching of the Smad signaling pathway induces precocious myogenic differentiation even in the presence of growth factors.

Id1 gene is one of the target genes of the Smad signaling pathway [27]. Its gene product, Id1, inhibits transcription of the MyoD family and suppresses terminal myogenic differentiation [37]. Id1 expression was inhibited in Ric10 cells exclusively in the central region even in pmGM (Fig. 4D), although Id1 is normally expressed in a serum-dependent manner (Fig. 3B) [37]. Similar expression patterns of phosphorylated Smad1/5/8 and Id1 imply that inactivation of the Smad signaling pathway may induce myogenin expression and myogenesis through suppression of Id1 expression.

Furthermore, differentiation-inducing culture for 24 h in pmDM following 24 h of culture in pmGM triggered the robust

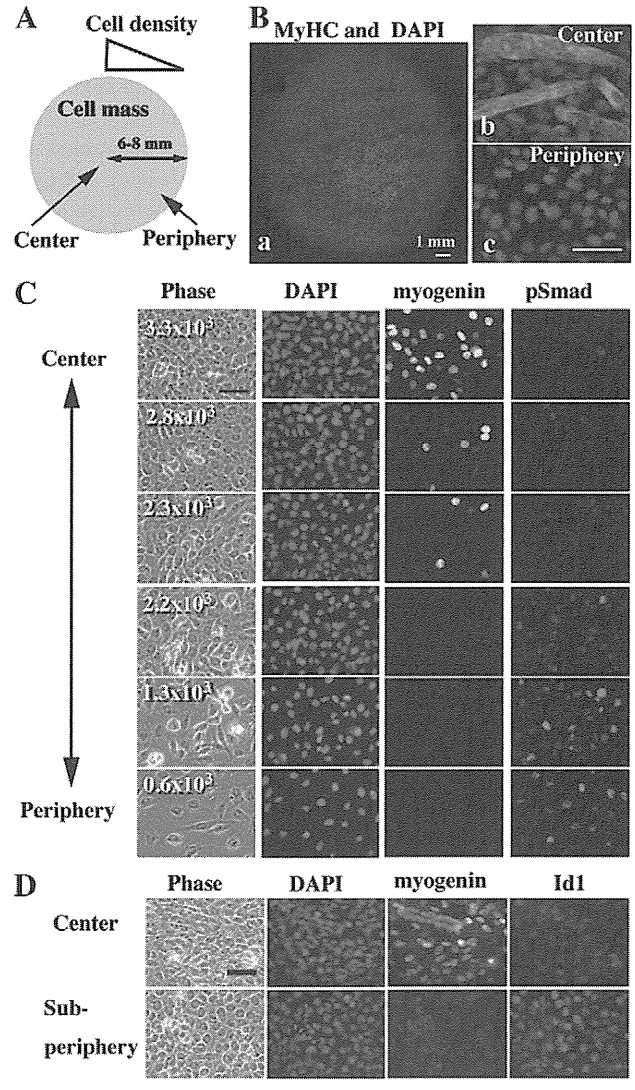

Fig. 4 – Down-regulation of phosphorylated Smad and Id1 during myogenesis triggered in high cell density culture. (A and B) For a micromass culture, 1×10^5 Ric10 cells were plated in a 100-μl spot and cultured in pmGM for up to 48 h. A diagram of micromass culture shows that cell density is reduced along with the center–periphery axis (A). MyHC was detected with a specific antibody (red) and nuclei were stained with DAPI (blue) in (B). Pictures show whole cell mass (a) and regions of center (b) or periphery (c). Scale bars, 1 mm (a) and 50 μm (b and c). (C and D) Ric10 cells (5×10^4 cells per 100-μl spot) were cultured in micromass for 48 h in pmGM. The cells were subjected to immunostaining with anti-myogenin and anti-pSmad or anti-Id1 antibodies. Nuclei were stained with DAPI. The numbers in phase contrast images in (C) represent the cell density of the indicated field (cells per mm^2). Images in each row were obtained from the same field. Scale bars: 50 μm.

expression of myogenin from the center to the sub-periphery of the cell mass (Fig. 5A). Ric10 cells gave rise to myotubes in the sub-peripheral region as well as the central region of the micromass. Serum reduction caused a rapid fall in the amount of phosphorylated Smad1/5/8 in micromass cultures (Fig. 5A). Id1 was down-

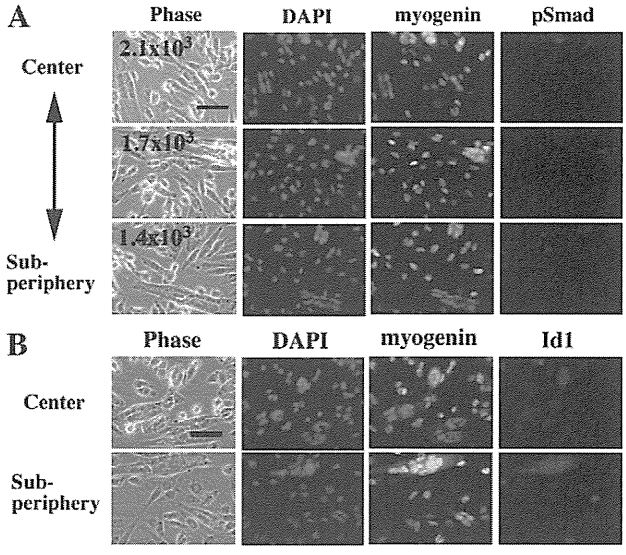

Fig. 5 – Synergistic induction of robust myogenesis by high cell density and serum reduction. (A and B) Ric10 cells (5×10^4 cells per 100 μl of spot) were cultured in micromasses in pmGM for 24 h and then further cultured in pmDM for up to 24 h. The cells were subjected to immunostaining with anti-myogenin, anti-pSmad, and anti-Id1 antibodies. Nuclei were stained with DAPI. The numbers in the phase contrast images in (A) represent cell density of the indicated field (cells per mm^2). Images in each row show the same field. Scale bars: 50 μm.

regulated even in the peripheral region of the micromass in pmDM (Fig. 5B). It should be noted that the cell density in the peripheral region of the micromass ($4–6\times10^2$ cells per mm^2) was still much higher than that of the low cell density cultures shown in Figs. 2 and 3 (less than 100 cells per mm^2). The results indicate that high cell density and serum reduction synergistically induced robust myogenic differentiation, possibly through quenching the Smad signaling pathway.

Dorsomorphin enhances myogenic differentiation in a cell density-dependent fashion under growth condition

To determine whether the Smad signaling pathway is involved in the regulation of myogenic differentiation induced in the high cell density culture, Ric10 cells were cultured in micromass under the growth condition and treated with dorsomorphin for 24 h after seeding. Myotube formation was markedly enhanced by dorsomorphin in a dose-dependent fashion (Fig. 6A). Expressions of MyHC and myogenin were also enhanced by dorsomorphin in a similar manner (Fig. 6B). Myotubes were robustly formed in both dorsomorphin-treated and untreated cultures when the cells were cultured for the prolonged period (48–60 h). The result indicates that dorsomorphin induced myogenic differentiation precociously.

In the next series of experiments, various numbers of Ric10 cells were cultured in micromass to understand whether cell density affects the enhancement of myogenesis by dorsomorphin. The highest concentration of cells in the central region of the cell mass increased along with the number of plated cells (Fig. 6C). Phosphorylation of Smad1/5/8 was suppressed in high cell density cultures (Fig. 6D). Dorsomorphin also inhibited phosphorylation of Smad1/5/8 and markedly enhanced myogenic differentiation in high cell density culture whereas its effects were obscure in relatively lower cell density culture (Fig. 6E). Dorsomorphin continuously but limitedly decreased the level of phosphorylated Smad1/5/8 per nucleus (Fig. 6F). Dorsomorphin and high cell density synergistically down-regulated phosphorylation of Smad1/5/8. When the concentration of phosphorylated Smad1/5/8 fell below the putative threshold that is represented by an arrow in Fig. 6F, expression of myogenin was induced (Fig. 6G). Dorsomorphin-treatment also resulted in down-regulation of Id1 and up-regulation of MyoD (Supplementary Fig. S3). These results imply that down-regulation of the Smad signaling pathway induces myogenic differentiation even in pmGM under the high cell density culture condition. Similar results were obtained from another mouse myogenic cell line, COM3, that was re-cloned from C2C12 cells (Supplementary Figs. S4–6) [23].

BMP antagonist noggin triggers myogenic terminal differentiation in a cell density-dependent fashion under growth condition

To determine whether precocious cell density-dependent, serum concentration-independent myogenic differentiation is suppressed by ligand BMP, Ric10 cells cultured in micromass were exposed to a BMP antagonist, noggin. The expression of MyHC and myogenin were induced in the center of cell mass exclusively (Fig. 7A). Recombinant noggin (5 mg/ml) enhanced myotube formation and the expression of MyHC and myogenin in the region with the relatively lower cell density (Fig. 7B). However, noggin failed to induce MyHC expression in Ric10 cells in the peripheral region where cell density was lower than 1000 cells per mm^2 (Fig. 7C). Consistent with the results in myogenesis assay, noggin decreased the level of phosphorylated Smad1/5/8 (Fig. 7D). The results suggest that ligand-dependent activation of the Smad signaling pathway contributes to the suppression of precocious differentiation of myogenic cells.

Smad signaling pathway is transiently activated in myogenic progenitor cells during muscle regeneration in vivo

To examine the involvement of the Smad signaling pathway in postnatal muscle regeneration, the phosphorylation of Smad1/5/8 was determined in regenerating muscle. Muscle regeneration was induced by injection of BPV into the gastrocnemius muscle of rats. During the early phase of muscle regeneration, myogenic progenitor cells derived from muscle satellite cells express MyoD but not myogenin in BPV-injected rat muscle. Then, the cells are induced to express both MyoD and myogenin, and they give rise to myofibers [38] (Umeda and Hashimoto, unpublished observation). We detected phosphorylated Smad1/5/8 in more than 50% of nuclei of MyoD-expressing myogenic cells in regenerating muscle on days 3 and 4 after BPV injection (Fig. 8Aa–d). A fraction of the myogenin-positive myogenic cells also showed phosphorylated Smad1/5/8 in their nuclei (Fig. 8Ae–h), but the percentage of phosphorylated Smad1/5/8-positive cells in the myogenin-positive mononucleated cells was less than that in the number of MyoD-positive mononucleated cells (39% vs. 65%). The results indicate that the Smad signaling pathway is first activated and then inactivated in myogenic progenitor cells during postnatal muscle regeneration. Therefore, the Smad signaling pathway may be involved in the regulation of growth and

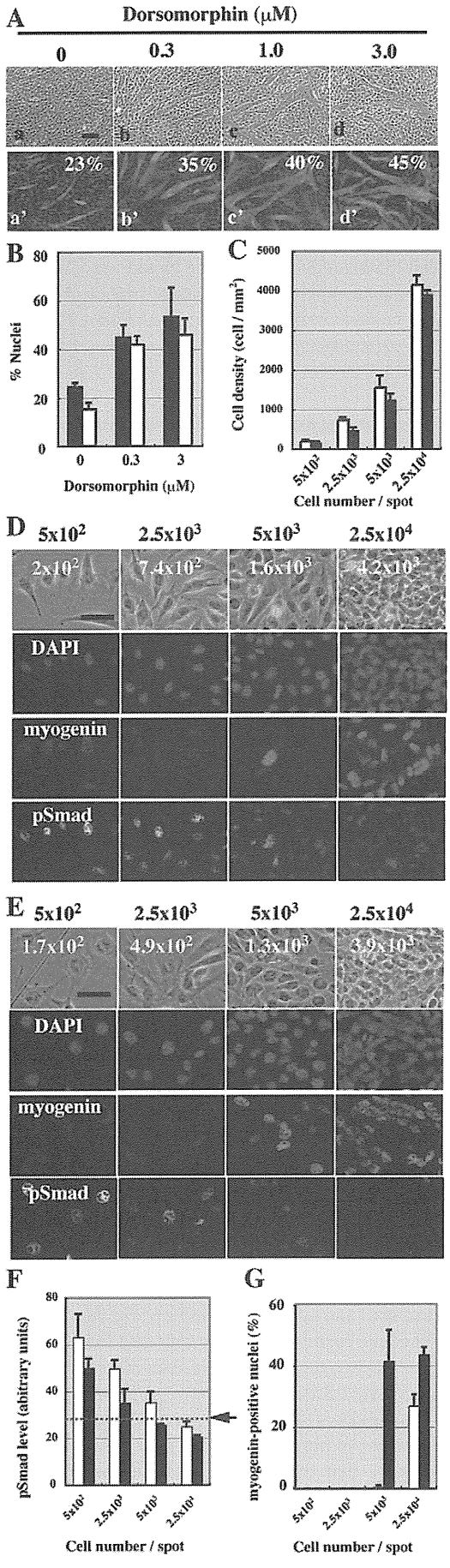

differentiation of postnatal myogenic cells in vivo as well as in vitro.

Discussion

Smad signaling pathway determines cell fates of myogenic cells

In the present study, we provide evidence for a novel role of the BMP–ALK–Smad axis in the switch between growth and differentiation of myogenic cells during postnatal muscle growth and repair. Autonomous cell expression of BMP receptors and downstream Smad proteins in postnatal myogenic cells implies a physiological function of the BMP–ALK–Smad axis during postnatal muscle differentiation. Actually, growing undifferentiated myogenic cells show significant activation of the Smad signaling pathway without administration of any exogenous BMPs. Four independent methods of blocking the BMP–ALK–Smad axis demonstrated that this physiological Smad signaling suppresses precocious differentiation of myogenic cells and keeps their undifferentiated state (Fig. 8B): inhibition of BMP function by noggin, inhibition of ALK2 activation by dominant negative ALK2, inhibition of the interaction between Smad1/5/8 and Smad 4 or ALK2 by an inhibitory Smad, and inhibition of phosphorylation of

Fig. 6 – Induction of precocious myogenic differentiation by dorsomorphin. (A and B) Ric10 cells (5×10^4 cells per 100-μl spot) were cultured in micromass in pmGM for 24 h and then further cultured in pmGM with (Ab–d) or without (Aa) dorsomorphin for up to 24 h. Each medium contained 0.03% DMSO. The cells were subjected to immunostaining with anti-MyHC alone (A) or anti-myogenin and anti-MyHC antibodies (B). Nuclei were stained with DAPI. Images of central regions of micromasses with the highest cell density were obtained by phase contrast (Aa–d) and epifluorescent microscopy (Aa′–d′). The percentages of nuclei in MyHC-positive cells in the total number of nuclei are shown in the lower panels (Aa′–d′). The percentages of nuclei in myogenin- and MyHC-positive cells in the total number of nuclei were calculated, and averages and standard deviations of three independent cultures are shown as solid and open bars, respectively in (B). (C–G) The indicated numbers of Ric10 cells per 50-μl spot were cultured in micromass in pmGM for 24 h and then further cultured in pmGM with 3 μM dorsomorphin (E and solid bars in C, F and G) or without (D and open bars in C, F and G) for up to 24 h. The cells were subjected to immunostaining with anti-myogenin and anti-pSmad antibodies. Nuclei were stained with DAPI. Images of the central regions of micromasses with the highest cell density were obtained by phase contrast (top panels) and epifluorescent microscopy (lower panels) in (D and E). Cell density (cells per mm^2) at the end of culture was calculated and is shown as averages and standard deviations of three independent cultures (C), or represented as numbers in the top panels (D and E). The relative concentration of pSmad in nuclei (F) and the percentages of myogenin-positive nuclei in the total number of nuclei (G) were calculated, and averages and standard deviations of three independent cultures are shown. Scale bars: 10 μm.

Smad1/5/8 by a protein kinase inhibitor dorsomorphin. The correlation between the levels of phosphorylated nuclear Smad1/5/8 and myogenin indicates a threshold of the Smad signal intensity that is sufficient to maintain myogenic cells in an undifferentiated state (Fig. 6F). When the level of Smad signaling is below the threshold, myogenic progenitor cells begin to undergo terminal myogenic differentiation (Fig. 8B).

Our previous study suggests that the exposure to high concentrations of BMP2 causes extraordinary activation of the Smad signaling pathway resulting in induction of osteogenesis in myogenic cells [9]. Hyper-activated Smad1/5/8 irreversibly prevents myogenesis, whereas spontaneously activated Smad1/5/8 suppresses precocious myogenic differentiation reversibly without exposure to exogenous BMPs. Then, hyperactivation of the Smad signaling pathway results in expression of Smad target genes that are not induced during myogenesis but are required for osteogenesis (Fig. 8B).

Recently, we found that high concentrations of BMPs induce ectopic osteogenesis of Ric10 in a cell density-dependent fashion (Supplementary Fig. S7). The results suggest a continuum in the effect of BMPs between the inhibition of myogenic differentiation and transdifferentiation into an osteogenic cell fate. In addition, low concentrations of BMP2 induced osteogenesis in Ric10 cells at low cell density (Supplementary Figs. S7B and C). Taken together with the Supplementary results, the magnitude of Smad signaling might play a critical role in generation of different fates from myogenic progenitor cells (Fig. 8B). In addition, we have found that the exogenous BMP-induced osteogenesis is facilitated by a co-signal (Yanagisawa and Hashimoto, unpublished). Therefore, cellular context and co-signals may determine whether a given BMP stimulus induces which cell fates. From this point of view, it is very interesting that the migrating Ric10 cells at the margin of a cell mass were refractory when exposed to high concentrations of BMP2 (Supplementary Figs. S7D and E).

Quenching of Smad signaling is rate-limiting for myogenic differentiation

The present study indicates that quenching of the Smad signaling pathway triggers myogenic differentiation under the high cell density culture condition. Serum reduction also lowered the phosphorylation level of the Smad signaling pathway. However, high cell density was more potent for inactivating the Smad signaling pathway than low serum concentration in the medium. The present study shows that the Smad signaling pathway is also rate-limiting for myogenic differentiation induced by serum reduction. However, the enhancement of myogenic differentiation by dorsomorphin was quite limited under the serum-reduced, low cell density culture condition. Thus, it is likely that distinct

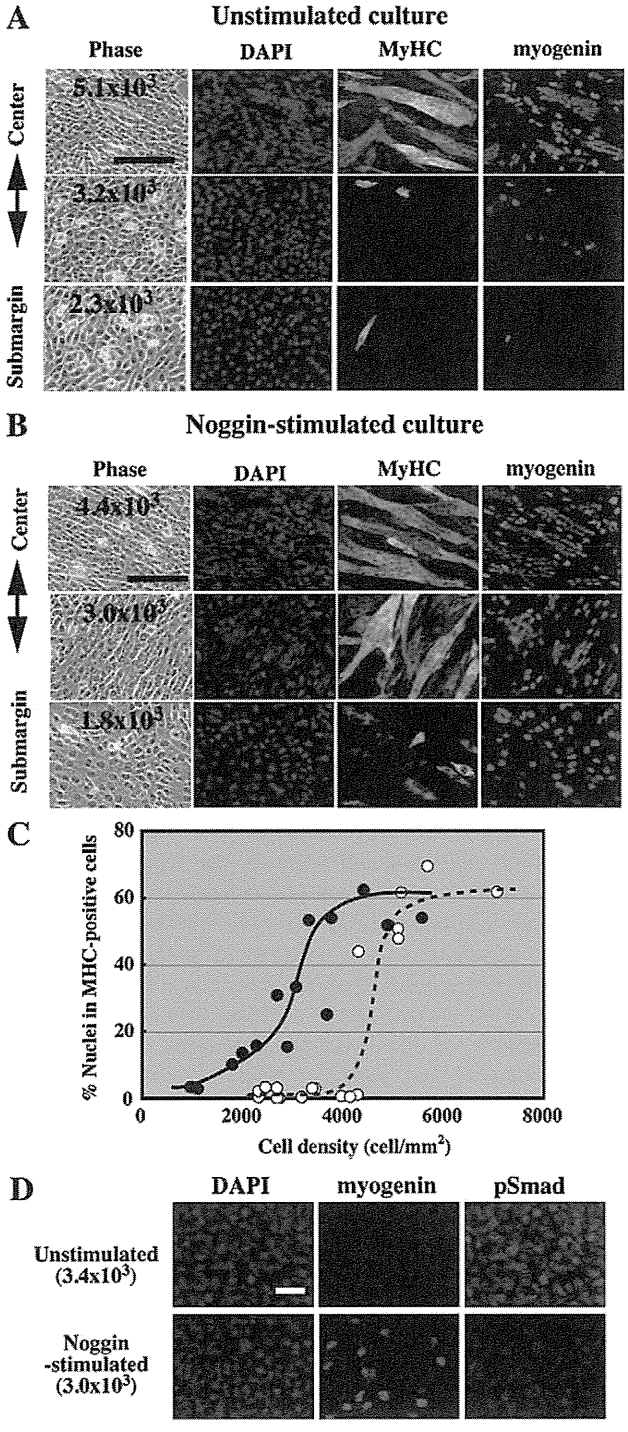

Fig. 7 – Induction of precocious myogenic differentiation by BMP antagonist noggin. (A, B and C) Ric10 cells (5×10^4 cells per 100-μl spot) were cultured in micromasses in pmGM for 24 h and then further cultured in pmGM with (B) or without (A) noggin (5 mg/ml) for up to 24 h. The cells were subjected to immunostaining with anti-myogenin and anti-MyHC antibodies. Nuclei were stained with DAPI. Images of various regions were obtained by phase contrast and epifluorescent microscopy. Numbers in the left-hand panels in A and B represent cell density (cell per mm^2). (C) Cell density and the percentages of nuclei in MyHC-positive cells in the total number of nuclei were calculated in cultures stimulated with (solid circles) or without (open circles) noggin. (D) Ric10 cells (5×10^4 cells per 100-μl spot) were cultured in micromasses in pmGM for 24 h and then further cultured in pmGM with (lower panels) or without (upper panels) noggin (5 mg/ml) for up to 24 h. The cells were subjected to immunostaining with anti-myogenin and anti-phosphorylated Smad1/5/8 antibodies. Nuclei were stained with DAPI. Images were obtained by epifluorescent microscopy. The numbers in parentheses at the left of panels represent cell density (cell per mm^2) at the end of culture. Scale bars: 50 μm.